Geospatial Based Analysis for Soil Erosion Susceptibility Evaluation: Application of a Hybrid Decision Model

[1]Chris C. Okonkwo, [13]Emmanuel C. Chukwuma, [1]Louis C. Orakwe, [2]Gloria C. Okafor

[1]Department of Agricultural and Bioresources Engineering, Faculty of Engineering,

Nnamdi Azikiwe University, Awka, Nigeria

[2]Department of Meteorology and Climate Change, Nigeria Maritime University, Okerenkoko Warri, Delta State, Nigeria

[3]Research Fellow, Future Africa Institute, University of Pretoria, South Africa

Corresponding author: Emmanuel C. Chukwuma;

Email: ec.chukwuma@unizik.edu.ng

Declarations

Conflict of interest: The authors declare that they have no known competing financial interests or personal relationships that could have appeared to influence the work reported in this paper.

CREDIT author statement

This work was carried out in collaboration between all the authors. Authors **E. C. Chukwuma** and **C. C. Okonkwo** designed the study, **C. C. Okonkwo** carried out the field survey and collected the data, **C. C. Okonkwo** and **E. C. Chukwuma** analyzed the data, wrote the protocol. **L. C. Orakwe** and **G. C. Okafor** wrote the first draft of the manuscript, **and** edited the manuscript.

Funding: This research did not receive any specific grant from funding agencies in the public, commercial, or not-for-profit sectors.

Data Availability: Data will be made available on request.

Code Availability: This does not apply to this manuscript.

Abstract

Erosion hazard is a major environmental change in developing countries and therefore necessitates investigations for effective erosion control measures. This study is hinged on the numerous advantages of a hybrid Multi-Criteria Decision Model (MCDM) to assess erosion vulnerability using remote sensed data and the application of Geographical Information System (GIS). Nine risk factors of erosion were selected for this study and their thematic maps were utilized to produce a spatial distribution of erosion hazard in the state. An integrated IVFRN-DEMATEL-ANP model was used to investigate the interrelationships between the risk factors and also obtain their final weights. The assessment model identified Rainfall, Erosivity Index, Stream Power Index, Sediment Transport Index, Topographic Wetness Index and Soil as the most influential factors of erosion in the study area. The weighted linear combination method was used to integrate the risk factors to produce the spatial distribution of erosion vulnerability model. The method was validated using Anambra State of Nigeria. The findings from the study revealed that Anambra State is vulnerable to erosion hazard with 45% of the state lying between Very High and Medium vulnerable zones. A good predictive model performance of 89.7% was obtained using the AUC-ROC method. The feasibility of integrating the IVFRN, DEMATEL and ANP models as an assessment model for mapping erosion vulnerability has been determined in this study and this is vital in managing the impact of erosion hazards globally. The model's identification of hydrological and topographical factors as major causes of erosion hazard emphasizes the importance of critical analysis of risk factors as done in this study for effective management of erosion. This study is a veritable tools for implementation of erosion mitigation measures.

Keywords: Erosion hazard, Vulnerability assessment, Geospatial analysis, Decision model, Anambra State of Nigeria

Introduction

Soil erosion is a major environmental, economic and social issue that constitutes land degradation and soil productivity loss which hampers the sustainable development of rural areas as well as the stability and health of the general society (Igwe et al. 2017). The problem of soil erosion is expected to increase due to climate change as the erosion process is largely influenced by variations in extreme precipitation (Eekhout & Vente 2022; Peng et al. 2022). The phenomenon of erosion is mainly attributed to the action of floods or running water and it can be described as a process that involves the detachment, transportation and deposition of soil particles by water, rainfall, and runoff (Isife 2019; Mushi et al. 2019). While there are four agents of soil erosion, i.e., water, wind, gravity, and freeze-thaw, however, 50% of global soil erosion is caused by water (Guo et al. 2019). Based on the nature of occurrence, soil erosion can generally be classified into two distinct categories. The first is a normal process that takes place for millions of years and leads to the formation of new soils, while the second is an accelerated process caused by anthropogenic activities such as deforestation, overgrazing, and unsuitable

farming practices which lead to more soil loss than soil formation (Ahmad et al. 2020). The second category is a major cause for concern as global population growth has resulted in a continual transformation of vast areas of natural vegetation into areas for human use, mainly for agricultural expansion (Xiong et al. 2019). Accelerated soil erosion has a negative effect on soil and crop productivity via reduction of nitrogen, phosphorus, and soil organic matter content; varying clay content of the soil; depletion of available water capacity; and the reduction of soil aggregation (Chalise et al. 2019). Other significant impacts of soil erosion on the environment include water quality degradation as a result of eutrophication in water bodies, siltation, increased flood risk, etc (Das et al. 2020). In addition to the land degradation caused by the detachment, the transported particles also affect human activities via the sedimentation of reservoirs for irrigation and drinking water purposes, and the destruction of housing and infrastructures (Eekhout & Vente 2022). The deposition of the transported particles in waterways can also lead to difficulties in navigation (Mushi et al. 2019).

Soil erosion is an evident environmental issue in the Southeastern part of Nigeria as it has destroyed various life forms, properties, transportation and communication systems, arable lands, surface and groundwater sources (Egboka et al. 2019; Egwuonwu et al. 2019). Anambra state is one of the worst-hit erosion states in South-East Nigeria with over 500 active erosion sites which cut across several rural communities in the state (Egwuonwu et al. 2019; Nwobodo et al. 2018). The issue of erosion in the state has attracted a lot of study and research. Mezie & Nwajuaku (2020) investigated the causes of gully erosion in some parts of Aguata local government area of the state and attributed the cause of erosion in the area to human activities as well as the inherent soil properties. In the upper Idemili River catchment of Anambra State, Nigeria, Chibuzor et al. (2020) observed that the porous and permeable nature of the soil, as well as its high hydraulic conductivity, triggered the development of gully erosion in the area. Iliyasu et al. (2019) studied the environmental effects of gully erosion in the Nanka community of Anambra state and observed that erosion in the area is caused by both natural and anthropogenic factors which include road construction without drainage, deforestation, disposal of solid waste in waterways, rainfall intensity and nature of soil among others. The study also identified the destruction of residential infrastructures, the loss of lives and farmlands, and psychological trauma as the effects of erosion in the area. Consequently, an investigation that enhances decision-making in mitigating the impact of soil erosion is critical for the study area

The applications of geospatial technologies such as GIS, spatial interpolation techniques, and the ever-growing range of environmental data in recent times have increased the importance of soil erosion modeling in the plan and execution of soil management and conservation strategies (Borrelli et al. 2021). To effectively and efficiently tackle soil erosion and its associated environmental issues, there is a need to identify areas prone to erosion for the

implementation of measures that are essential for the conversation of soil resources and the restoration of ecological systems (Guo et al. 2021). The accessibility of remotely sensed data, developmental strides in computation, and the incorporation of data in GIS have facilitated the mapping and identification of areas vulnerable to erosion where conservation is highly needed (Tamene & Le 2015). Furthermore, the Spatio-temporal variations in soil erosion due to variations in climate, soil, topography, vegetation, and conservation measures (Jin et al. 2021), make GIS an ideal tool for its assessment. GIS is a very useful tool in developing automated methods for measuring the spatial variability of hazard and erosion-related issues, and it is largely employed in supporting modeling and hazard analysis (Rahman et al. 2015). With the aid of GIS, several machine learning tools have been employed for the assessment of various hazards. Mosavi et al. (2022) employed a Generalized Linear Model (GLM), Flexible Discriminate Analyses (FDA), Multivariate Adaptive Regression Spline (MARS), Random Forest (RF), and their ensemble to assess erosion and flood susceptibility in Iran. Mosavi et al. (2020) also studied soil erosion susceptibility using Weighted Subspace Random Forest (WSRF), Gaussian Process with a Radial Basis Function Kernel (Gaussprradial), and Naive Bayes (NB) methods. Amongst the various models which can be supported by GIS in vulnerability assessment, the multi-criteria decision-making (MCDM) model has gained attention in the study of hazard vulnerability. This can be attributed to the use of GIS to visualize and spatially analyze geographic data to support the environmental decision-making process (Saini et al. 2015). Furthermore, the combination of the multi-criteria decision-making (MCDM) models with GIS also helps to improve the decision-making process. The MCDM models can be used to identify vulnerable areas to erosion by evaluating different alternatives based on certain criteria (Halefom et al. 2018). The identification of the main factors which influence soil erosion is very important when considering the implementation of natural restoration policies (Guo et al. 2021). The application of GIS and the MCDM models makes it possible to combine the spatial values of alternatives and the weights of criteria to identify the best option (Arabameri et al. 2019).

Various MCDM models have also been investigated for the assessment of erosion hazard vulnerability in Nigeria. Dike et al. (2015) evaluated the vulnerability of the Urualla watershed to soil erosion based on a multi-criteria technique of AHP. The model was used to assess the criteria of rainfall, soil, topography, land cover, and conservation practice. Igwe et al. (2020) employed the Analytical Hierarchy Process (AHP) models to assess areas prone to gully erosion in Gombe town and environs based on ten predisposing factors of erosion which include elevation, slope angle, curvature, aspect, topographic wetness index (TWI), soil texture, geology, drainage buffer, road buffer and land-use. In Anambra state, Odunuga et al. (2018) examined the susceptibility of the Orashi River Basin (ORB) to soil erosion. While the MCDM models have been employed in the vulnerability assessment of erosion hazards, a major limitation that exists with these models is the fact that they do not address the uncertainty which might occur in the decision-making process (Haidara et al. 2019). To address this limitation,

researchers over the years have hybridized the MCDM models with other methods to improve the reliability of the decision-making process. In hazard vulnerability assessment, some of these methods used in the hybridization of the MCDM models include the Fuzzy Logic (Haidara et al. 2019; Saha et al. 2019), Interval Rough Numbers (Pamucar et al. 2017; Hatefi & Tamošaitienė 2019; Wang et al. 2019), Interval Value Fuzzy Rough Numbers (IVFRN) (Pamučar et al. 2018), etc.

Sajedi-Hosseini et al. (2018) assessed soil erosion susceptibility in Iran using the Fuzzy-DEMATEL-ANP method and obtained an accuracy of 83.4%. The study relied on the Fuzzy method to overcome uncertainty and vagueness in human preferences, whereas this present study seeks to employ the IVFRN method to do the same. In recent years, the IVFRN method has emerged as a more improved algorithm due to its ability to combine the advantages of both the Fuzzy and the Rough Numbers algorithms without retaining their disadvantages. The use of IVFRN owing to its advantages was employed in this study. It is important to state that the application of the IVFRN algorithms is a critical research area, but it has not been fully harnessed in Nigeria. Despite the benefits of hybridization of the MCDM models for erosion vulnerability assessment, it is yet to be utilized for better decision making in the study area as previous works for the study area utilized solely GIS or simplified decision models as stated above. To the best of the author's knowledge, no study has investigated erosion vulnerability in the study area with a strong emphasis on the integration of decision models to eliminate the limitation of a single decision model as done in this study. The integration of various decision models with geospatial technology is therefore pertinent in the production of enhanced soil erosion geospatial models, for better decision-making in tackling the impact of erosion particularly for an erosion-prone zone of Southeast Nigeria.

Hence this study aims to explore the hybridization of MCDM models in the assessment of erosion vulnerability in a geospatial setting. The study seeks to hybridize the Analytic Network Process (ANP) method by integrating it with the Decision Making Trial and Evaluation Laboratory (DEMATEL) and the IVFRN methods. The IVFRN method is an algorithm that handles imprecision and uncertainties contained in decision-making. Rather than relying on models of any assumption, the algorithm relies on internal knowledge from the data and employs objective indeterminacy to make decision-making possible (Pamučar et al. 2019). The DEMATEL method was developed by Gabus and Fontela of the Battelle Memorial Institute of Geneva and it was developed between 1972 and 1976 (Song et al. 2020). The method has been widely accepted as one of the best methods in the decision-making process for creating and examining the relationships between factors and their influences on the overall system (Kadoic et al. 2019). The ANP method can be described as a general form of the AHP method whereby the decision-making process is structured as a network rather than a hierarchy (Kadoic et al. 2019). In contrast to the AHP, the ANP doesn't depend on a hierarchical structure but employs a

feedback-based system to address the problem (Hatefi & Tamošaitienė 2019). The objective of this study is to integrate the three aforementioned models for an efficient and effective decision-making process in mitigating soil erosion. This is very important as the study will provide data on the most vulnerable areas to erosion threats which will ensure risk-based spatial planning toward the conservation and restoration of environmental resources.

Study area

Anambra state is a south-eastern state in Nigeria that is located between longitudes 6˚ 35′ and 7˚ 50′ East and latitudes 5˚ 40′ and 6˚ 48′ North. The state (study area) and its Local Government Areas (LGAs) are shown in Figure 1 below. The state has a human population that is estimated to be over 6 million (Obioji & Eze 2019). There are two significant landforms in the state which consist of the low-lying regions that are in the western, northern, and north-eastern parts of the state, and the high-lying regions that are in the southern part (Okoyeh et al. 2014). There are two major climatic seasons in the state and this include the rainy season which spans from April to September and the dry season which spans from October to March (Enekwechi 2017). Furthermore, climate change effect has greatly disrupted the start and end of the two major climatic seasons in the state (Okoyeh et al. 2014).. Heavy and abundant rainfall can be observed in the state during the rainy season with an annual rainfall that ranges from 1400 mm to 2500 mm and increasing from the northern part of the state to the southern part (Fagbohun et al. 2017).

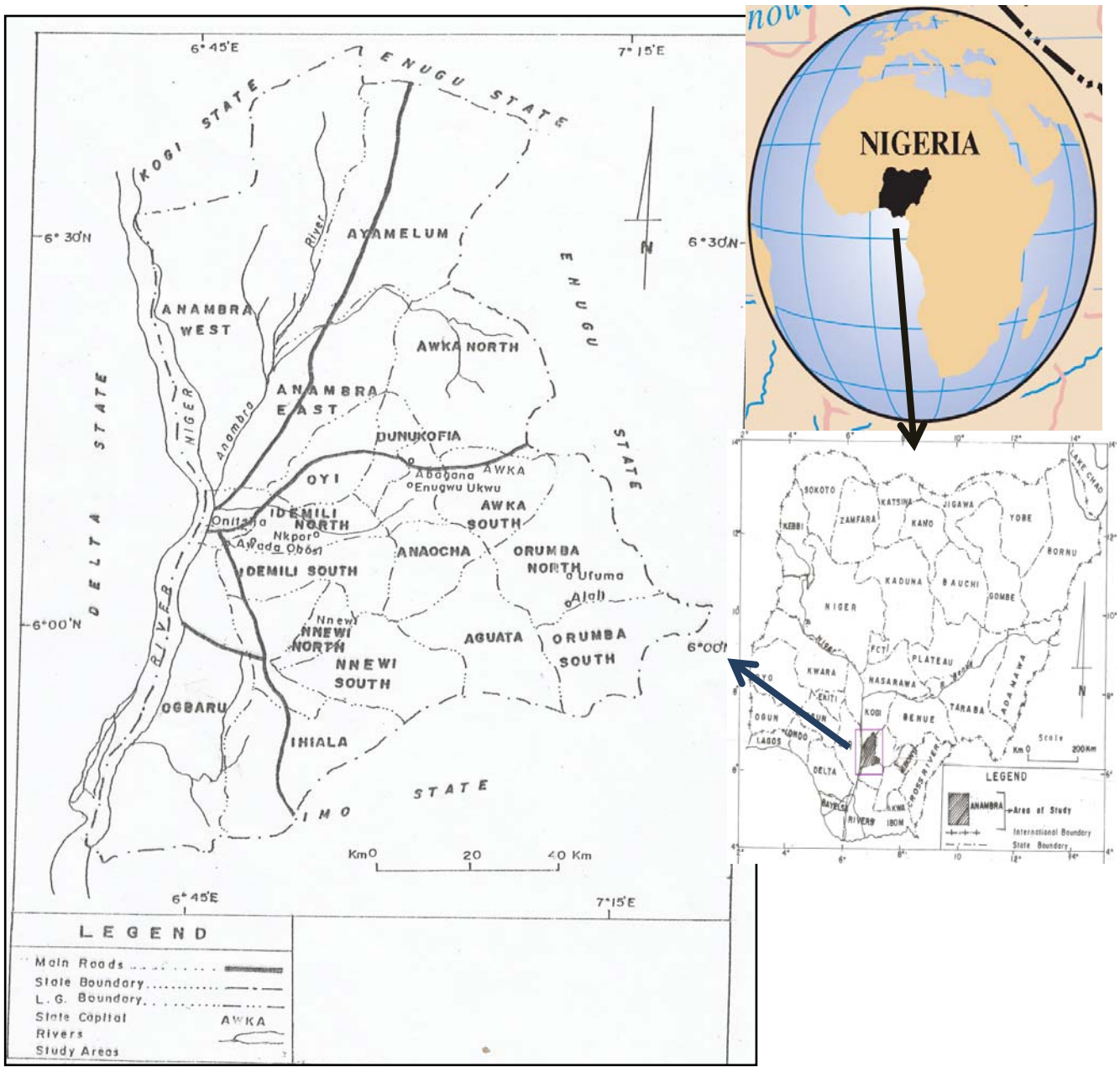

Figure 1: Map of the Study Area

Data and methods

To assess erosion vulnerability, this study relied on 9 (nine) conditioning factors or criteria and these include Rainfall Erosivity Index (C_1), Stream Power Index, SPI (C_2), Sediment Transport Index, STI (C_3), Topographic Wetness Index, TWI (C_4), Soil (C_5), Land Use (C_6), Normalized Difference Vegetation Index (C_7), Slope (C_8) and Elevation (C_9). The various steps which were

taken to integrate the risk factors to accomplish the goal of this study are shown in the methodological flowchart in Figure 2. This section further discusses the hybrid MCDM model and the processes employed to assess erosion vulnerability in the study area. To produce the thematic map layers of the risk factors, application of GIS was utilized. Furthermore, the interrelationship between the risk factors and their influence in inducing erosion hazard was examined using the IVFRN-DEMATEL-ANP model and their final weight subsequently obtained. Finally, the Weighted Linear Combination (WLC) method was employed to produce a spatial distribution of erosion hazard vulnerability in the study area.

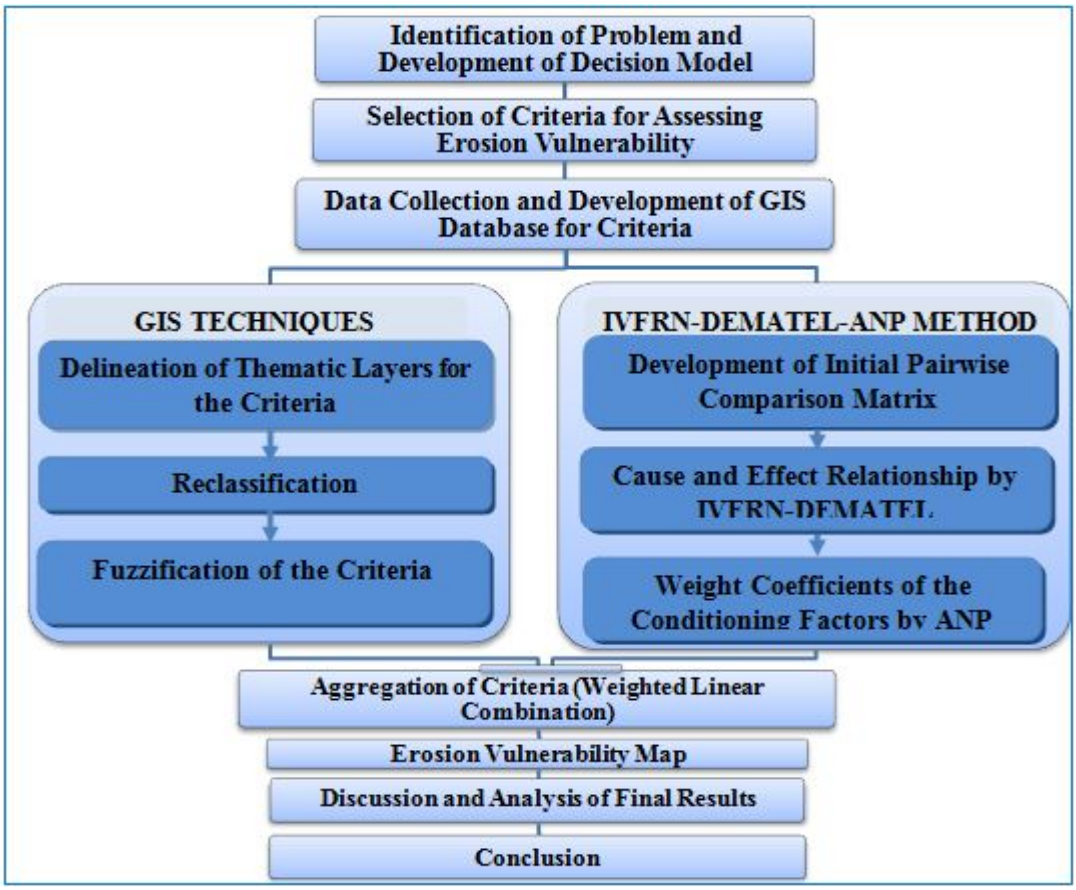

Figure 2: Flowchart of the Study's Methodology

Data collection and analysis

The average annual rainfall data of the study area covering a period of 26 years (1991-2016) was obtained from Worldbank's climate database. The data obtained was used to calculate the Rainfall Erosivity Index factor as shown in equation 1 below.

$$REI = \sum_{i=1}^{12} 1.735 \times 10^{\left[1.5 \log_{10}\left(P_i^2/P\right) - 0.08188\right]}$$

(1)

Where P_i represents the average for i-th month and P is the annual average rainfall (Kanani-Sadat et al. 2019). The data was imported into the GIS environment to delineate the thematic layer map for the Rainfall Erosivity Index factor. The study area's Digital Elevation Model (DEM) was collected from the Shuttle Radar Topography Mission (SRTM) instrument provided by the United States Geological Survey (USGS) and this data was used to produce the slope and elevation maps of the study area. The TWI factor which measures the accumulation of water in soil due to slope and upstream catchment area was calculated from the DEM using equation 2.

$$TWI = ln(A_s / \tan\beta)$$

(2)

where A_s is the upstream contributing area and β is the slope gradient (in degrees).

The SPI factor which measures the erosive power of flowing water, was calculated from the DEM using equation 3

$$SPI = A_s \times \beta$$

(3)

The STI factor was also calculated from the DEM using equation 4

$$STI = (m+1) \times (A_s/22.13)^m \times \sin(\beta/0.0986)^n$$

(4)

Soil data of the study area was obtained from the Harmonized World Soil Database (HWSD) by Food Agriculture Organization (FAO) and data was used to produce the soil map of the study area. Three Landsat 8 Operational Land Imager (OLI) imageries covering the study area was obtained from the United State Geological Survey (USGS) website

Table 1 Landsat 8 images of the study area

and this was used to produce the landuse map of the study area.

Table 1 Landsat 8 images of the study area

LANDSAT 8 IMAGES	PATH/ROW	DATE
1	189/55	1 February 2018
2	189/56	1 February 2018
3	188/56	27 December 2018

The NDVI factor map was obtained from the Landsat 8 imagery of the study area using equation 5 below.

$$NDVI = \frac{IR - R}{IR + R} \quad \textbf{(5)}$$

Where IR is the infrared portion of the electromagnetic spectrum (Band 5) and R is the red portion of the electromagnetic spectrum (Band 4).

Based on their influence on erosion hazard occurrence, the conditioning factors for erosion vulnerability assessment were classified into various fuzzy memberships. This was done to form a basis for their comparison. The risk factors that had categorical values such as the land use and soil map layers were reclassified into numeric values before putting them into fuzzy membership class. Two fuzzy membership classes of Fuzzy Gaussian and the Fuzzy Large were employed for the analysis as shown in Table 2. The Fuzzy Gaussian function is used when the midpoint value is most likely to cause a hazard. In a situation where high input values of a risk factor are the most likely to induce a hazard, the Fuzzy Large function is employed (Okonufua et al. 2019).

Table 2 Fuzzy membership class of the risk factors for erosion vulnerability assessment

RISK MAPS	INITIAL VALUES	RESOLUTION	FUZZY MEMBERSHIP
Rainfall Erosivity Index	79, 919.69531 — 82, 587.55156 82, 587.55157 — 85, 255.40781 85, 255.40782 — 87, 923.26406 87, 923.26407 — 90,591.12031 90,591.12032 — 93,258.97656	1 : 78,000	Fuzzy Large
SPI	-5.567567825 — -0.588114712 -0.588114712 — -0.187980087 -0.187980087 — 0.034316927 0.034316927 — 0.256613941 0.256613941 — 5.769579887	30m	Fuzzy Large
STI	0 — 41.47129672 41.47129673 — 311.0347254 311.0347255 —1,161.196308 1,161.196309 — 3,131.082902 3,131.082903 — 5,287.590332	30m	Fuzzy Large
TWI	3.602589607 — 7.31942648 7.319426481 — 9.30173948 9.301739481 —11.77963073 11.77963074 — 15.00088935 15.00088936 — 24.66466522	30m	Fuzzy Large
Soil	Fluvisol = 5 Nitrosol = 4 Plinthosol = 3 Gleysol = 2 Alluvial = 1	1 : 78,000	Fuzzy Large
Slope (degree)	0 — 1.363358801 1.363358802 — 3.578816851 3.578816852 — 6.475954303 6.475954304 — 11.2477101 11.24771011 — 43.45706177	30m	Fuzzy Large
Elevation (m)	313 — 388 238 — 313 163 — 238 88 — 163 13 — 88	30m	Fuzzy Large
Land Use	Agriculture = 5 Barren Land = 4 Urban = 3 Forest = 2 Water = 1	30m	Fuzzy Large
NDVI	-0.091505267 — 0.01907845 0.01907845 — 0.105088008 0.105088008 — 0.155991624	30m	Fuzzy Gaussian

	0.155991624 — 0.203384646 0.203384646 — 0.356095493		

Erosion assessment model

The proposed hazard assessment model in this study employs a GIS MCDM structure, taking advantage of the applicability of GIS in managing geospatial data and the flexibility of MCDM to integrate spatial hydrological and topographical information with value-based information (survey) (Hategekimana et al. 2018; Wang et al. 2019). The model integrates the three methods of IVFRN, DEMATEL, and ANP in a step by step process to determine the weight of the risk factors. The first step involves the use of the IVFRN method to eliminate uncertainty in the decision-making process. In the second step, a network of relationship between the conditioning factors of erosion hazard is created and their degree of influence in the system is examined using the DEMATEL method. In the third step, the ANP method is employed to determine the individual weight of the risk factors. Finally, the WLC method is applied to produce a spatial model of the vulnerability of erosion in the study area. This section goes further to give a detailed description of the steps.

Application of the IVFRN method

The IVFRN method can generally be described as the use of an initial reference fuzzy set to define uncertainties in the decision-making process and the use of rough sets to analyze these uncertainties (Pamučar et al. 2018). The IVFRN method is the combination of both the traditional fuzzy set and the rough number set in such a way that their benefit is retained while eliminating their drawbacks (Roy et al. 2020). For more information on the IVFRN method and its mathematical equations, please see (Pamučar et al. 2018).

The required input data for application of the IVFRN method is the initial pairwise comparison matrix which is provided by experts. A triangular fuzzy number $A_{ij}^{k} = \left(l_{ij}^{k},\ m_{ij}^{k},\ n_{ij}^{k}\right)$ is used for evaluation where k depicts the number of participating experts in which k = 1……..N. The decision of k-th expert regarding the effect of i-th criterion on j-th one is A_{ij}^{k}. For this study, three (3) experts in erosion mitigation study participated in the questionnaire survey and the

questionnaire distributed employed the predefined fuzzy scale shown in Table 3 for evaluation. A sample of the questionnaire and the obtained responses are shown in the appendix.

Table 3 Linguistic values and their corresponding fuzzy triples (Source: Kanani-Sadat et al. 2019)

Linguistic values	Triple Fuzzy Numbers
Very High Influence (VH)	(0.75, 1.0, 1.0)
High Influence (H)	(0.5, 0.75, 1.0)
Low Influence (L)	(0.25, 0.5, 0.75)
Very Low Influence (VL)	(0, 0.25, 0.5)
No Influence (NO)	(0, 0, 0.25)

The obtained initial pairwise comparison matrix which constitute of triangular fuzzy numbers l_{ij}^k, m_{ij}^k, n_{ij}^k was transformed into rough sequences $RS(l_{ij}^k)$, $RS(m_{ij}^k), RS(n_{ij}^k)$ (see appendix). Where $RS(l_{ij}^k) = [\underline{Lim}\,(l_{ij}^k),\ \overline{Lim}\,(l_{ij}^k)]$, $RS(m_{ij}^k) = [\underline{Lim}\,(m_{ij}^k),\ \overline{Lim}\,(m_{ij}^k)]$, $RS(n_{ij}^k) = [\underline{Lim}\,(n_{ij}^k),\ \overline{Lim}\,(n_{ij}^k)]$. $\underline{Lim}\,(l_{ij}^k)$, $\underline{Lim}\,(m_{ij}^k)$ and $\underline{Lim}\,(n_{ij}^k)$, represent the lower limits and $\overline{Lim}\,(l_{ij}^k)$, $\overline{Lim}\,(m_{ij}^k)$ and $\overline{Lim}\,(n_{ij}^k)$ represent the upper limit of the rough sequences $RS(l_{ij}^k)$, $RS(m_{ij}^k), RS(n_{ij}^k)$.

The next step in the IVFRN method is the aggregation of the rough sequence of all the decision-makers and this is done by applying equations 6, 7 and 8 below.

$$RS(\bar{l}_{ij}) = RS(l_{ij}^1, l_{ij}^2, \dots, l_{ij}^k) \begin{cases} \bar{l}_{ij}^L = \dfrac{1}{M}\sum_{k=1}^{M} l_{ij}^{kL} \\ \bar{l}_{ij}^U = \dfrac{1}{M}\sum_{k=1}^{M} l_{ij}^{kU} \end{cases} \quad \textbf{(6)}$$

$$RS(\overline{m}_{ij}) = RS(m_{ij}^1, m_{ij}^2, \dots, m_{ij}^k) \begin{cases} \overline{m}_{ij}^L = \dfrac{1}{M}\sum_{k=1}^{M} m_{ij}^{kL} \\ \overline{m}_{ij}^U = \dfrac{1}{M}\sum_{k=1}^{M} m_{ij}^{kU} \end{cases} \quad \textbf{(7)}$$

$$RS(\overline{n}_{ij}) = RS(n_{ij}^1, n_{ij}^2, \ldots, n_{ij}^k) \begin{cases} \overline{n}_{ij}^L = \dfrac{1}{M}\sum_{k=1}^{M} n_{ij}^{kL} \\ \overline{n}_{ij}^U = \dfrac{1}{M}\sum_{k=1}^{M} n_{ij}^{kU} \end{cases}$$

(8)

where k refers to the kth expert (k = 1, 2,…, M), $RS(\overline{l}_{ij})$, $RS(\overline{m}_{ij})$and $RS(\overline{n}_{ij})$ denotes the rough sequences that collectively make up the IVFRN $\bar{\bar{d}}_{ij}$ = [($\overline{l}_{ij}^L$, $\overline{l}_{ij}^U$), ($\overline{m}_{ij}^L$, $\overline{m}_{ij}^U$), ($\overline{n}_{ij}^L$, $\overline{n}_{ij}^U$)]. Hence, the IVFRN decision matrix can be derived as $\overline{\overline{D}}$

$$\overline{\overline{D}} = \begin{bmatrix} \bar{\bar{d}}_{11} & \bar{\bar{d}}_{12} & \cdots & \bar{\bar{d}}_{1c} \\ \bar{\bar{d}}_{21} & \bar{\bar{d}}_{22} & \ldots & \bar{\bar{d}}_{2c} \\ \vdots & \vdots & \ddots & \vdots \\ \bar{\bar{d}}_{c1} & \bar{\bar{d}}_{c2} & \cdots & \bar{\bar{d}}_{cc} \end{bmatrix}_{c \times c}$$

(9)

Where c refers to the number of risk factors

The final step in the IVFRN method is the defuzzification of the IVFRN decision matrix to obtain our initial decision matrix. This was proposed by Kanani-Sadat et al. (2019), as a necessary means of understanding the relationship between the risk factors. Here we defuzzify the matrix $\overline{\overline{D}}$ using Equation 10 below to obtain the elements of our initial decision matrix D (Equation 11).

$$D_{ij} = \left(1 + \frac{\overline{l}_{ij}^L + \overline{n}_{ij}^U}{2}\right) \times \left(\frac{\overline{l}_{ij}^L + \overline{l}_{ij}^U + 2\overline{m}_{ij}^L + 2\overline{m}_{ij}^U + \overline{n}_{ij}^L + \overline{n}_{ij}^U}{8}\right)$$

(10)

$$D = \begin{bmatrix} D_{11} & D_{12} & \cdots & D_{1c} \\ D_{21} & D_{22} & \ldots & D_{2c} \\ \vdots & \vdots & \ddots & \vdots \\ D_{c1} & D_{c2} & \cdots & D_{cc} \end{bmatrix}_{c \times c}$$

(11)

Application of the DEMATEL method

The DEMATEL method utilizes graph theory to visualize the process of addressing a problem in such a way that all significant factors can be classified as a cause or an effect, thereby making it easier to understand the complex nature of the problem, the interrelationship between its factors, and the degree of influence of the factors (Pamucar et al. 2017). The input data for the DEMATEL method is the initial decision matrix D, which was derived from the IVFRN method.

In the first step of the DEMATEL method, we normalize the elements of the initial decision matrix D to obtain normalized matrix $\bar{\bar{Z}}$ as shown in Equation 12 below

$$\bar{\bar{Z}} = \begin{bmatrix} \bar{\bar{z}}_{11} & \bar{\bar{z}}_{12} & \cdots & \bar{\bar{z}}_{1c} \\ \bar{\bar{z}}_{21} & \bar{\bar{z}}_{22} & \ldots & \bar{\bar{z}}_{2c} \\ \vdots & \vdots & \ddots & \vdots \\ \bar{\bar{z}}_{c1} & \bar{\bar{z}}_{c2} & \cdots & \bar{\bar{z}}_{cc} \end{bmatrix}_{c \times c} \tag{12}$$

The elements $\bar{\bar{z}}_{ij}$ of the matrix $\bar{\bar{Z}}$ are derived using Equation 13 below.

$$\bar{\bar{z}}_{ij} = \frac{D_{ij}}{\lambda} \tag{13}$$

where λ is given by the equation: $\lambda = {1}\Big/{\max\limits_{1 \le i \le n} \left(\sum_{j=1}^{n} D_{ij} \right)}$ (14)

The next step in the DEMATEL method is to examine the total relationship between the conditioning factors illustrated by the matrix T which describes the direct and indirect relationships between the risk factors. The matrix T is calculated using Equation 15 and 16 below, where I is an Identity matrix.

$$T = \begin{bmatrix} t_{11} & t_{12} & \cdots & t_{1c} \\ t_{21} & t_{22} & \ldots & t_{2c} \\ \vdots & \vdots & \ddots & \vdots \\ t_{c1} & t_{c2} & \cdots & t_{cc} \end{bmatrix}_{c \times c} \tag{15}$$

$$t_{ij} \ = \ \bar{\bar{z}}_{ij} \times \left(I - \ \bar{\bar{z}}_{ij}\right)^{-1}$$

(16)

Next, we calculate the values of R and S, where R describes the direct and indirect effect that each factor i has on other factors. This is determined by computing the sum of the i-th row of the matrix T as shown in Equation 17 below. Also S describes the overall effect all other factors have on the j factor and this is determined by computing the sum of the j-th column of the matrix T as shown in Equation 18 below.

$$R = \ [R_i]_{c\times 1} = \sum_{j=1}^{c} t_{ij}$$

(17)

$$S = \ \left[S_j\right]_{1\times c} = \sum_{i=1}^{c} t_{ij}$$

(18)

The values of $R + S$ and $R - S$ are used to describe the importance of the various factors and understand the interrelationship between them. $R + S$ describes the degree of influence that factor i has on other factors and as such denotes its significance to the problem. $R - S$ on the other hand describes the influence the factor has in the system, with a positive value indicating that the i-th factor is effective and as such is categorized into "causes". Furthermore, obtaining a negative value of $R - S$ means that the i-th factor will be under the influence of other factors and as such is categorized into "effects". Factors that have high values of $R - S$ have greater priority than those with low values.

Application of the ANP method

In the ANP method, supermatrices are employed to examine the dependences of the risk factors and these supermatrices must be based on the principle of column stochastic, hence the

summation of elements in each column must be equal to 1 (Pamucar et al. 2017). The ANP method makes use of the total relationship matrix T as input data to determine the final weight of the risk factors. The application of the ANP method to determine the weight of the risk factors guarantees that the interdependence levels of factors are assessed as reciprocal values (Wang et al. 2019).

The first step in the ANP method is to create an unweighted supermatrix from the total relationship matrix T and this is done by defining an α-cut threshold to eliminate minor influences in the matrix T. The α-cut threshold is determined by experts and Equation 19 below shows the resultant matrix $T_{\propto}$. If $t_{ij} < \propto$ then ${t^{\propto}}_{ij} = 0$, otherwise ${t^{\propto}}_{ij} = t_{ij}$, where t_{ij} constitutes the elements of the matrix T.

$$T^{\propto} = \begin{bmatrix} t_{11}^{\propto} & \cdots & t_{1j}^{\propto} & \cdots & t_{1n}^{\propto} \\ \vdots & \vdots & \vdots & & \\ t_{i1}^{\propto} & \cdots & t_{ij}^{\propto} & \cdots & t_{in}^{\propto} \\ \vdots & \vdots & \vdots & & \\ t_{n1}^{\propto} & \cdots & t_{nj}^{\propto} & \cdots & t_{nn}^{\propto} \end{bmatrix} \quad \textbf{(19)}$$

The matrix $T^{\propto}$ gives us our unweighted supermatrix.

Next, we create a weighted supermatrix by normalizing the unweighted supermatrix $T^{\propto}$. To achieve this, we determine the sum of elements of the matrix $T^{\propto}$ by columns. The normalization of the matrix $T^{\propto}$ yields the elements of the matrix $\widetilde{W}$, which is our weighted super-matrix and the equation is given as:

$$\widetilde{W} = \begin{bmatrix} \widetilde{w}^{11} & \widetilde{w}^{12} & \cdots & \widetilde{w}^{1c} \\ \widetilde{w}^{21} & \widetilde{w}^{22} & \ldots & \widetilde{w}^{2c} \\ \vdots & \vdots & \ddots & \vdots \\ \widetilde{w}^{c1} & \widetilde{w}^{c2} & \cdots & \widetilde{w}^{cc} \end{bmatrix}_{c \times c} \quad \textbf{(20)}$$

Where $\widetilde{W}^{ij} = {t^{\propto}}_{ij}/\tilde{d}_i$, and the value of $\tilde{d}_i$ is obtained from $\tilde{d}_i = \sum_{i=1}^{n} {t^{\propto}}_{ij}$.

In the final step, the weights of the risk factors are determined by obtaining a limit super-matrix. This is done by multiplying the matrix $\widetilde{W}$ by itself multiple times or raising it to a power where the super-matrix converges and become a long-term stable super-matrix to obtain global priority vectors, called IVFRN-DEMATEL-ANP weights. This can be represented as $\lim_{k\to\infty} = \widetilde{W}^k$, where W refers to the limit super matrix and k refers to any power. After the determination of the individual weights of the conditioning factors, we aggregate them to produce our erosion vulnerability map.

Erosion vulnerability map

To obtain the erosion vulnerability map, the weighted linear combination method was employed to integrate the risk factors based on their relative weights. The equation of the weighted linear combination method is given below as

$$VI = \sum_{i=1}^{n} W_i C_i \quad \textbf{(21)}$$

Where VI represents the vulnerability index, W_i is represents the relative weight of each factor and C_i represents the relevant score of each factor which is the fuzzified map layer in this study. The resultant vulnerability index map was then categorized into five distinctive classes that consist of "very high", "high", "medium", "low" and "very low".

Results and discussion

Thematic Map Layers of the Criteria for Erosion Vulnerability Asessment

The risk factors considered for the purpose of this study were selected based on expert opinion, literature review and availability of data for the study area. These factors include Rainfall Erosivity Index, SPI, STI, TWI, Soil, Land Use, NDVI, Slope and Elevation. The necessary data for the investigation were obtained and processed through the application of GIS to produce the map layers of the risk factors. Figure 3 shows the fuzzified map layers of the risk factors for Erosion vulnerability assessement. The rainfall erosivity index observed in the study area varied from 79919 in Ayamelum LGA to 93258 in Orumba South and Ihiala LGAs. As a catalyst for

sheet and rill erosion, the rainfall erosivity index is a very important factor in assessing soil erosion with rainfall characteristics such as annual amount, seasonal distribution, and intensity having a huge influence on the erosion process (Saha et al. 2019). Higher rainfall erosivity index is associated with higher erosion risk, hence the rainfall erosivity index factor was fuzzified using the Fuzzy Large membership function and the obtained result is shown in Figure 3a. The SPI of the study area ranged from -5.5676 to 5.7696. The SPI factor describes the potential energy surface water has to erode soil particles and this energy is a function of the combinative effect of water flow path, flow accumulation and slope (Andualem et al. 2020). An increase in this energy leads to an increase in erosion risk, hence the SPI factor was fuzzified using the Fuzzy Large membership function and the resultant map is shown in Figure 3b. The STI factor measures the ability of the overland flow to transport soil particles and in the study area, STI values ranged from 0 to 5287.5903. Higher capacity to transport sediments indicate a higher risk of erosion as they tend to favour the erosion process, hence the Fuzzy Large membership function was used to standardize the STI factor and the resultant map is shown in Figure 3c. The TWI of the study area which describes the infiltration rate in the area ranged from 3.6025 to 24.6647. Higher values of TWI indicate a higher risk of erosion based on its potential to facilitate the development of piping and roof collapse (Bashir et al. 2020). As such, the TWI factor was fuzzified using the Fuzzy Large membership function and the fuzzified map is shown in Figure 3d.

The soil factor has a major influence on the erosion process as the development of subsurface flow and piping is dependent on the physical characteristics of the soil (Ogbonnaya et al. 2020). The soil map of the study area showed five classes of soil and these include Alluvial, Fluvisol, Plinthosol, Nitrosol and Gleysols. The soil map was further reclassified to create a basis for standardization utilizing numeric values that range from 1 to 5. Here, Fluvisol was given the highest numeric value of 5 as it is characterized by weak topsoil formation which favors the erosion process. Five classes of landuse were also delineated in the study area and these include water, forest, agricultural lands, barren lands and urban areas with agricultural and barren lands dominating most part of the state. The landuse factor plays a critical role in the erosion process as the geological stability of the slope is hugely influenced by landcover (Aslam et al. 2021). Furthermore, different types of landuse have different effect on the ability of rainfall to erode soil

particles as areas which experience soil disturbances and those with less vegetation tend to favor the erosion process. Based on this, the landuse map was also reclassified for standardization utilizing numeric values that range from 1 to 5. Here, agricultural lands were assigned the highest numerical value of 5. The membership function of Fuzzy Large was then utilized for fuzzifying the soil and landuse as shown in Figure 3e and Figure 3f for soil and landuse respectively. Vegetation plays a significant role in the erosion process as barren lands favor the erosion process by depriving soil surface the required protective cover against the erosive power of water. The NDVI is a vegetative factor which describes the greenness and healthiness of vegetation (Aslam et al. 2021). In the study area, the NDVI values ranged from -0.0915 to 0.3561. Negative values of NDVI refer to water and the positive values refer to shrubs, grassland, temperate and tropical rainforests while values near zero refer to barren areas (Aslam et al. 2021). Hence, the Fuzzy Gaussian membership function was used to fuzzify the NDVI factor and the result is shown in Figure 3g. The slope of the study area ranged from 0 to 43.457 degrees with a flat slope dominating the Northern part of the state and a steep slope dominating the Southern part of the state. The slope factor has an effect on soil erosion as runoff, drainage intensity and the removal of soil particles are largely influenced by steepness (Saha et al. 2019). The Fuzzy Large membership function was used to standardize the slope factor because steep slopes are more prone to erosion in comparison to flat slopes as more runoff occurs on them due to force of gravity. The result is shown in Figure 3h.

Elevation as integral factor in erosion vulnerability assessment determines the microsite's condition and influences the distribution of plants in the area such as their morphology, physiology and growth (Halefom et al. 2018). The elevation of the study area varied from 13m observed in the Northern part of the state to 388m observed in the Southern part of the state and the Fuzzy Large membership function was used for fuzzification as shown in Figure 3i. This is because areas with higher elevation are more prone to erosion as they are less likely to be protected by vegetation.

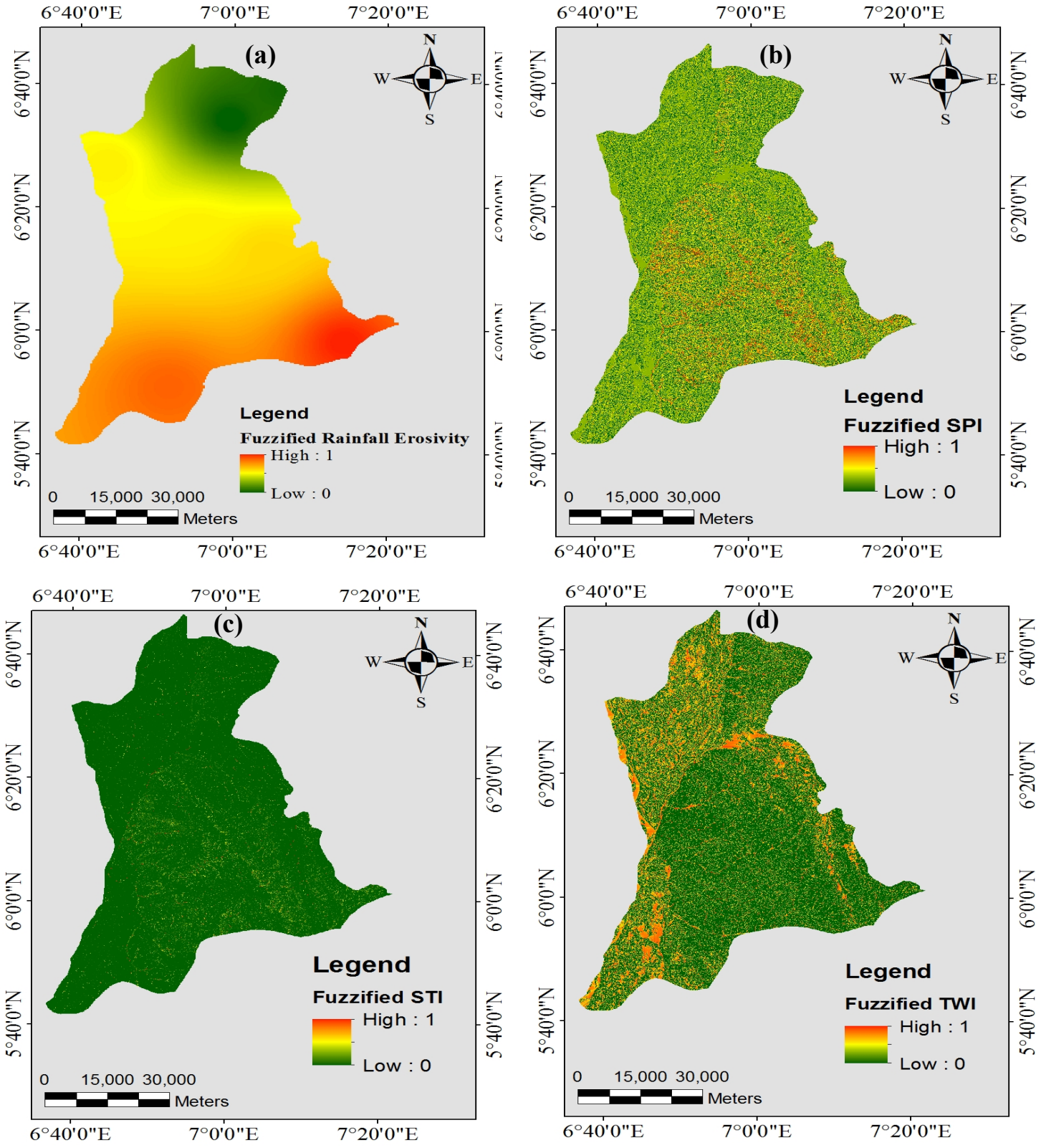

Figure 3: Conditioning Factors for Erosion Vulnerability Assessment. (a) Rainfall Erosivity Index; (b) SPI; (c) STI; (d) TWI; (e) Soil; (f) Landuse; (g) NDVI; (h) Slope; (i) Elevation

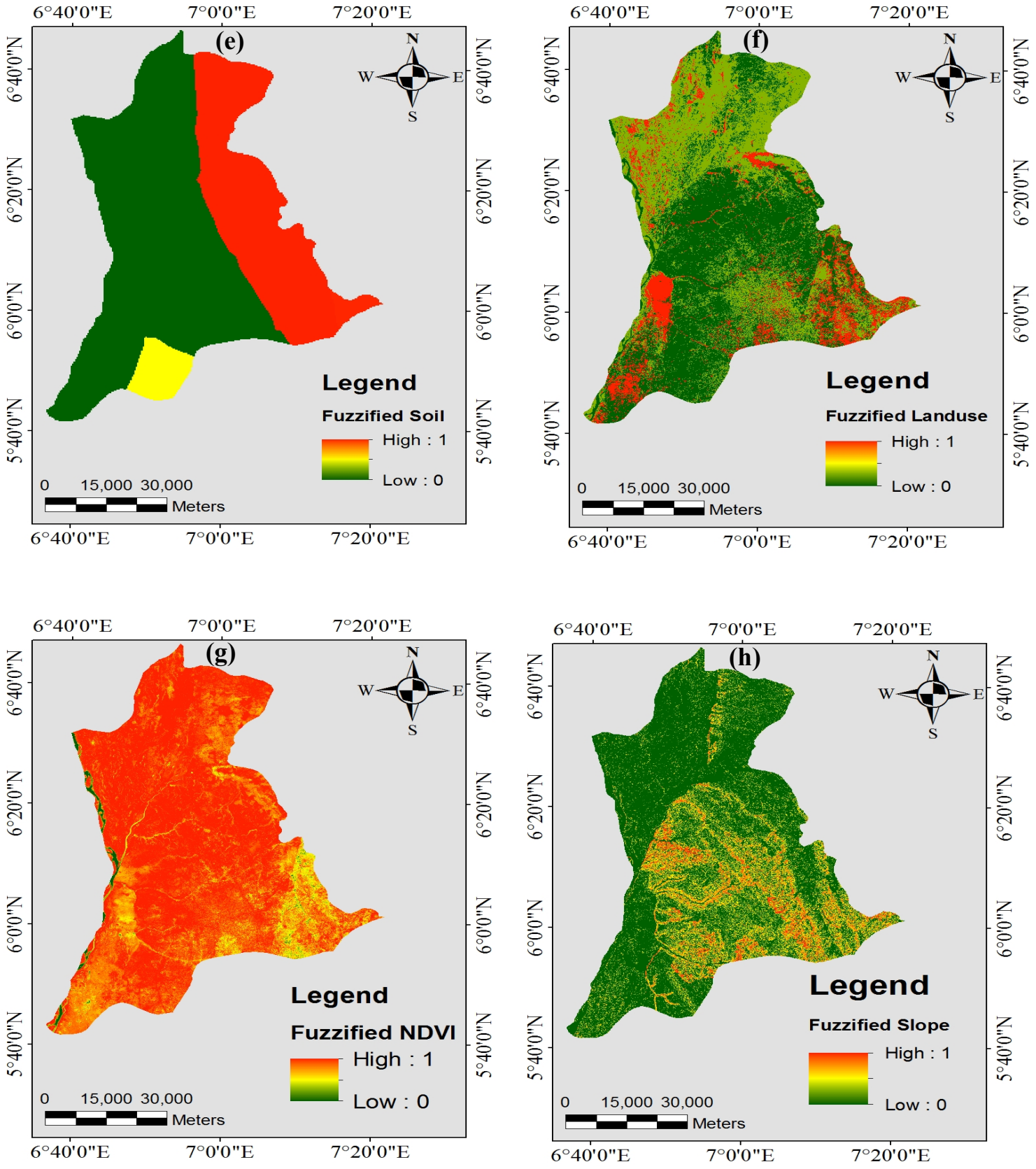

Figure 3: ***(continued)***

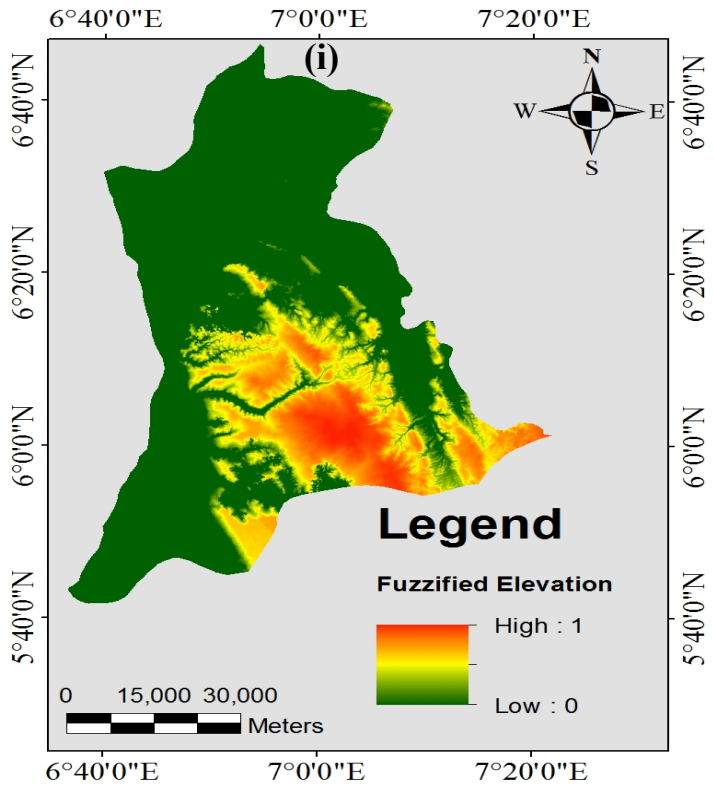

Figure 3. ***(continued)***

Determination of the interrelationship between risk factors

The interrelationship between the risk factors of erosion hazard was assessed and determined by integrating the IVFRN and DEMATEL methods was used to obtain the final weights of the various conditioning factors. The pairwise comparison matrix obtained through questionnaire survey was utilized as input data for the model. To eliminate the uncertainty and vagueness that exist in the decision making process, the triple fuzzy value of the initial pairwise comparison matrix was converted to Interval Value Fuzzy Rough Numbers. Then the average IVFRN matrix which represents our IVFRN decision matrix $\overline{\overline{D}}$ was derived by employing Equations 6, 7 and 8 to aggregate the IVFRN pairwise comparison matrix. To aid the interpretation of data, the IVFRN decision matrix was defuzzified using Equation 10 to produce the matrix D and the result is shown in

Table **4** below.

Table 4 Initial decision matrix

	C_1	C_2	C_3	C_4	C_5	C_6	C_7	C_8	C_9
C_1	0.07	0.76	0.93	0.76	0.59	0.93	0.44	1.06	1.58
C_2	0.76	0.07	0.93	0.93	0.76	0.76	0.76	1.58	1.44
C_3	0.44	0.46	0.07	0.93	1.01	1.32	1.11	1.44	1.58
C_4	0.34	0.34	0.34	0.07	1.11	1.11	0.90	1.44	0.93
C_5	0.15	0.34	0.34	0.34	0.07	0.57	0.90	1.44	1.58
C_6	0.34	0.44	0.44	0.44	0.44	0.07	1.44	1.44	1.58
C_7	0.15	0.44	0.44	0.44	0.44	0.44	0.07	0.59	0.75
C_8	0.46	0.75	0.75	0.75	0.46	0.93	0.46	0.07	1.44
C_9	0.46	0.75	0.75	0.75	0.46	0.46	0.46	0.46	0.07

Equation 12, 13 and 14 was then used to normalize the elements of our initial decision matrix to obtain the matrix $\bar{\bar{Z}}$. The matrix $\bar{\bar{Z}}$ was then used to calculate the total relation matrix T which describes the interrelationships between the risk factors. This was achieved using Equations 15 and 16 and the result is shown in Table 5 below.

Table 5 Total relationship matrix

	C_1	C_2	C_3	C_4	C_5	C_6	C_7	C_8	C_9
C_1	0.15	0.29	0.33	0.32	0.29	0.38	0.33	0.49	0.61
C_2	0.24	0.23	0.35	0.37	0.33	0.39	0.38	0.58	0.64
C_3	0.21	0.28	0.25	0.36	0.36	0.44	0.43	0.57	0.66
C_4	0.16	0.22	0.23	0.21	0.32	0.36	0.34	0.48	0.49
C_5	0.13	0.2	0.21	0.22	0.17	0.27	0.3	0.43	0.5
C_6	0.16	0.23	0.24	0.26	0.24	0.24	0.39	0.47	0.54
C_7	0.1	0.16	0.17	0.18	0.17	0.2	0.16	0.27	0.32
C_8	0.18	0.26	0.27	0.29	0.25	0.34	0.29	0.33	0.53
C_9	0.15	0.22	0.23	0.29	0.21	0.24	0.24	0.31	0.31

Equations 17 and 18 were used to calculate the rows (R) and the columns (S) of matrix T respectively and the result is shown in Table 6. This was done to assess the effect of each risk factor and their significance in inducing erosion hazard. The summation of the rows and columns of the matrix T gave values which describe the total direct and indirect effects that each risk factor received from and transferred to other risk factors. These values were further utilized to illustrated the complicated interrelationship between the risk factors by developing the CER diagram (see Figure 4 below), where the values of $\boldsymbol{R+S}$ are on the x axis and the values of $\boldsymbol{R-S}$ on the y axis.

Table 6 Values of importance and prominence

	$\widetilde{\boldsymbol{R}}$	$\boldsymbol{S}$	$\boldsymbol{R+S}$	$\boldsymbol{R-S}$
$\mathbf{C_1}$	3.19	1.48	4.67	1.71
$\mathbf{C_2}$	3.51	2.09	5.6	1.42
$\mathbf{C_3}$	3.56	2.28	5.84	1.28
$\mathbf{C_4}$	2.81	2.5	5.31	0.31
$\mathbf{C_5}$	2.43	2.34	4.77	0.09
$\mathbf{C_6}$	2.77	2.86	5.63	-0.09
$\mathbf{C_7}$	1.73	2.86	4.59	-1.13
$\mathbf{C_8}$	2.74	3.93	6.67	-1.19
$\mathbf{C_9}$	2.2	4.6	6.8	-2.4

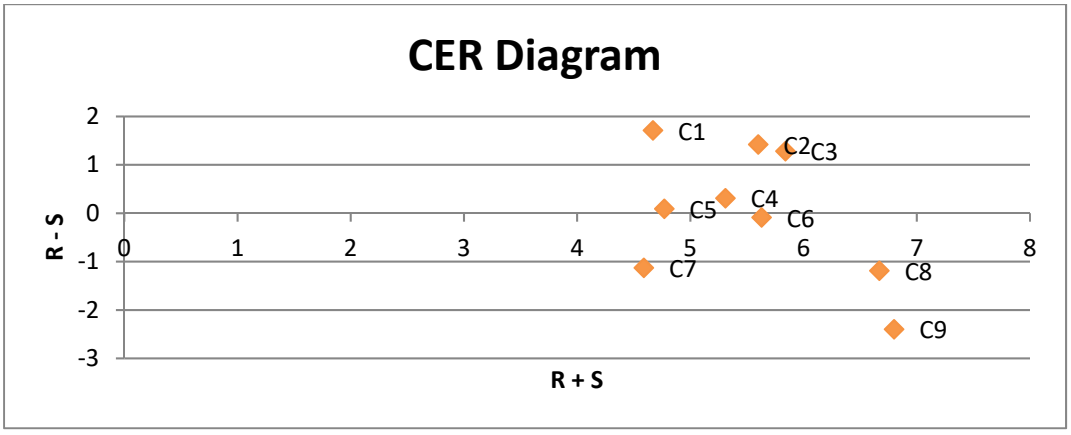

Figure 4: Cause and Effect Relationship (CER) Diagram of Conditioning Factors

The obtained values of $\boldsymbol{R-D}$ for erosion vulnerability assessment show that Rainfall Erosivity Index, Stream Power Index, Sediment Transport Index, Topographic Wetness Index and Soil are the main inducers of erosion hazard and fall into the cause group while Land Use, Normalized Difference Vegetation Index, Slope, and Elevation are under the influence of the other risk factors and as such are classifed into the effect group. Rainfall Erosivity Index has the most significant effect with the highest positive value of 1.71 and Elevation is under the most effect with the highest negative value of -2.4. This signifies that with respect to erosion hazard process, the erosive power of rainfall has the greatest effect on other risk factors while elevation is affected the most by other factors. This can be attributed to heavy rainfall normally experienced in the study area with average rainfall that vary from 1400mm to 2500mm annually.

Determination of final weights of risk factors

Using the total relationship matrix obtained from the DEMATEL method as input data, the ANP method was employed to determine the relative weights of the risk factors. Firstly, we obtained an unweighted supermatrix by averaging the experts opinion regarding the optimum α threshold to arrive at a value of 0.02. All the values in the total relation matrix less than the threshold value were equated to 0 in matrix T, hence the unweighted supermatrix matrix $T^{\propto}$ was derived. Equation 20 was then used to normalize the matrix $T^{\propto}$ to obtain the weighted supermatrix $\widetilde{W}$ and the result is shown in Table 7 below. Finally, to obtain the weight of the conditioning factors, the weighted supermatrix $\widetilde{W}$ was raised to the power of 8 to limit it and produce convergent values which are the relative weights of the risk factors (Table 8). The obtained relative weights of the risk factors for erosion vulnerability assessment show that SPI has the greatest priority with a final weight of 0.1941, followed by STI, Rainfall Erosivity, Slope, TWI, Landuse, Elevation, Soil and NDVI with final weights of 0.1851, 0.1245, 0.1057, 0.1018, 0.0996, 0.0880, 0.0810 and 0.0203 respectively. This indicates that SPI, STI, Rainfall Erosivity Index, Slope and TWI are the most significant risk factors for assessing the vulnerability of the study area to erosion hazard.

Table 7 Weighted supermatrix

	C_1	C_2	C_3	C_4	C_5	C_6	C_7	C_8	C_9
C_1	0.0000	0.1503	0.1564	0.1379	0.1450	0.1329	0.1222	0.1247	0.1326
C_2	0.5333	0.1192	0.1659	0.1595	0.1650	0.1364	0.1407	0.1476	0.1391
C_3	0.4667	0.1451	0.1185	0.1552	0.1800	0.1538	0.1593	0.1450	0.1435
C_4	0.0000	0.1140	0.1090	0.0905	0.1600	0.1259	0.1259	0.1221	0.1065
C_5	0.0000	0.1036	0.0995	0.0948	0.0000	0.0944	0.1111	0.1094	0.1087
C_6	0.0000	0.1192	0.1137	0.1121	0.1200	0.0839	0.1444	0.1196	0.1174
C_7	0.0000	0.0000	0.0000	0.0000	0.0000	0.0699	0.0000	0.0687	0.0696
C_8	0.0000	0.1347	0.1280	0.1250	0.1250	0.1189	0.1074	0.0840	0.1152
C_9	0.0000	0.1140	0.1090	0.1250	0.1050	0.0839	0.0889	0.0789	0.0674

Table 8 Relative weights of risk factors

Conditioning Factor	Final Weight
Rainfall Erosivity (C_1)	0.1245
SPI (C_2)	0.1941
STI (C_3)	0.1851
TWI (C_4)	0.1018
Soil (C_5)	0.0810
Landuse (C_6)	0.0996
NDVI (C_7)	0.0203
Slope (C_8)	0.1057
Elevation (C_9)	0.0880

Production of erosion vulnerability map

The various conditioning factors were integrated using the weighted linear combination method to produce the erosion vulnerability map. The fuzzified map layers of the various conditioning factors were integrated into the GIS environment using the raster calculator function. The obtained erosion vulnerability index map was further classified into five distinct categories of "very high", "high", "medium", "low" and "very low" using the classification methods of "Natural Breaks". Figure 5 shows the produced erosion vulnerability map of the study area as well as its Local Government Areas (LGA). The study area occupies a land mass of about 4559 sq km. The erosion vulnerability map revealed that 966.23 sq km, which represent 21% of the study area falls into very low vulnerable zone, 1555.05 sq km (34%) falls into low vulnerable zone, 1188.74 sq km (26%) falls into medium vulnerable zones, 664.60 sq km (15%) falls into highly vulnerable zones and 184.85 sq km (4%) falls into very high vulnerable zone. Very high vulnerable to medium vulnerable zones were mainly observed in the southern part of the state. This conforms with the work of Ajibade et al. (2020), which observed high erosion vulnerability that extend from the central part of the state to the southern part with towns such as Agulu, Nanka, Oko and Ekwulobia amongst the most vulnerable towns. With respect to land mass, the LGA most vulnerable to erosion hazard in the state is Orumba North with 290.97 sq km which represents 81% of the total Orumba North area lying between Very High and Medium Vulnerable zones. The second most vulnerable LGA is Orumba South with 218.44 sq km which represents 96% of the total Orumba South area lying between Very High and Medium Vulnerable zones. Other notable vulnerable LGAs to erosion hazards in Anambra State include Ayamelum, Awka South, and Awka North. In these LGAs, the high vulnerability to erosion hazard observed can be largely attributed to heavy rainfall recorded in the area, the topography of these areas where steep slopes dominate and the high rate of agricultural activities. High rainfall occurring on a steep slope of fluvisol will favor the erosion process and the development of gullies. This is due to a lack of cohesion between soil particles which makes their detachment by rainfall easier. Furthermore, the maximum gravitational force is provided by the slope for the subsequent transportation of sediment load in suspension or solution by transforming potential energy to kinetic energy (Bashir et al. 2020).

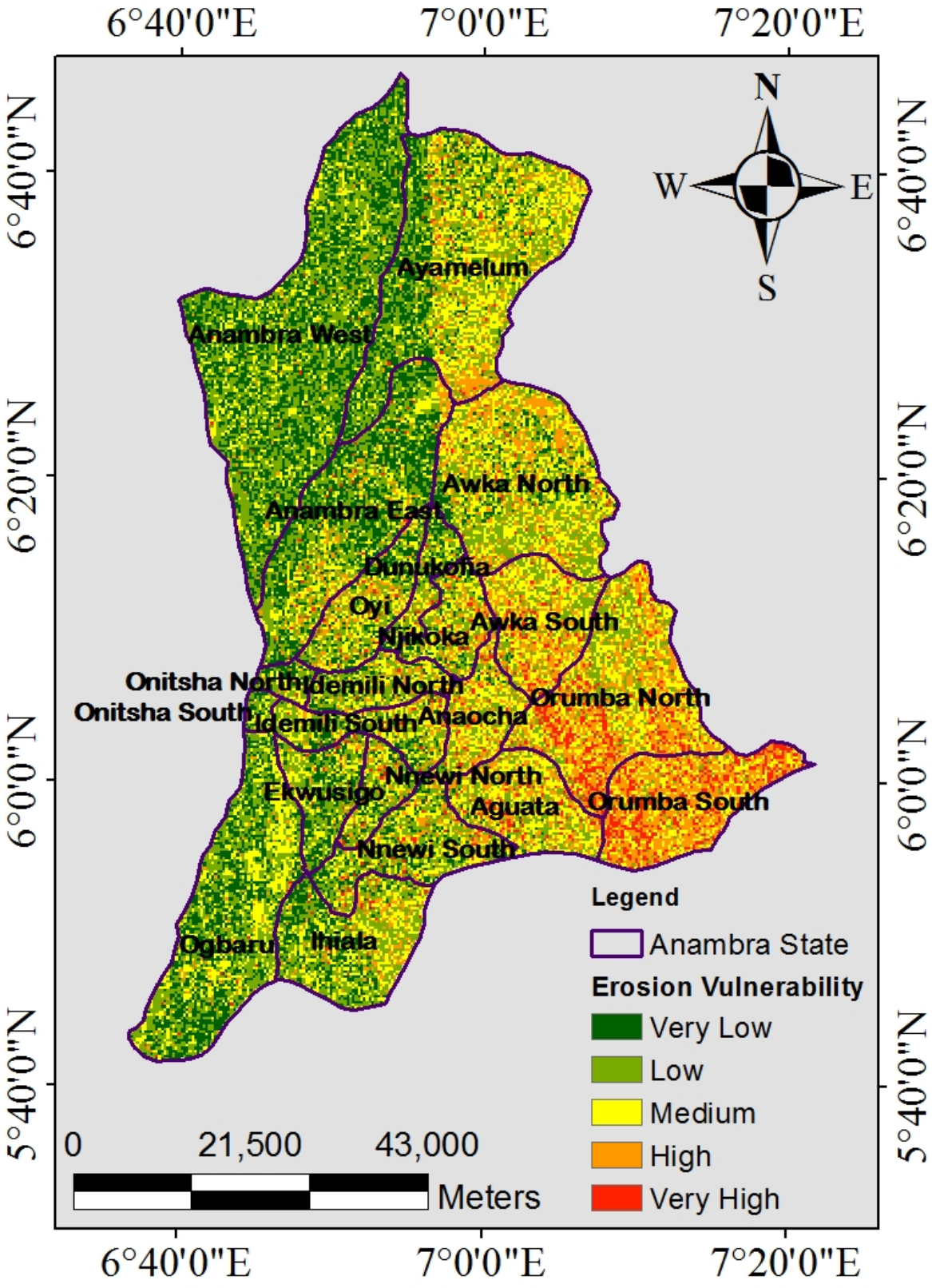

Figure 5: Erosion Vulnerability Map of the Study Area Showing the LGAs

Validation of the erosion vulnerability assessment model

Validation of assessment models is a very important aspect of vulnerability assessment as it is used to determine the predictive performance of the assessment model. Amongst the various methods available for validating assessment models, the area under the curve (AUC) of the receiver operating characteristics (AUC-ROC) has been widely used and accepted. Hence this study uses the AUC-ROC method to determine the predictive performance of the IVFRN-DEMATEL-ANP method. The AUC-ROC method signifies the ability of the assessment model to predict predetermined occurrences or non-occurrences. To apply the AUC-ROC, geospatial location of erosion features were obtained from the field survey and imported into the GIS environment. The result of the validation is shown in Figure 6 below. An AUC value of 0.897 was obtained for the IVFRN-DEMATEL-ANP model which shows that the model has an accuracy of 89.7% for soil erosion prediction in the study area. According to the classification by Yesilnacar (2005), this indicates that the model has good predictive performance.

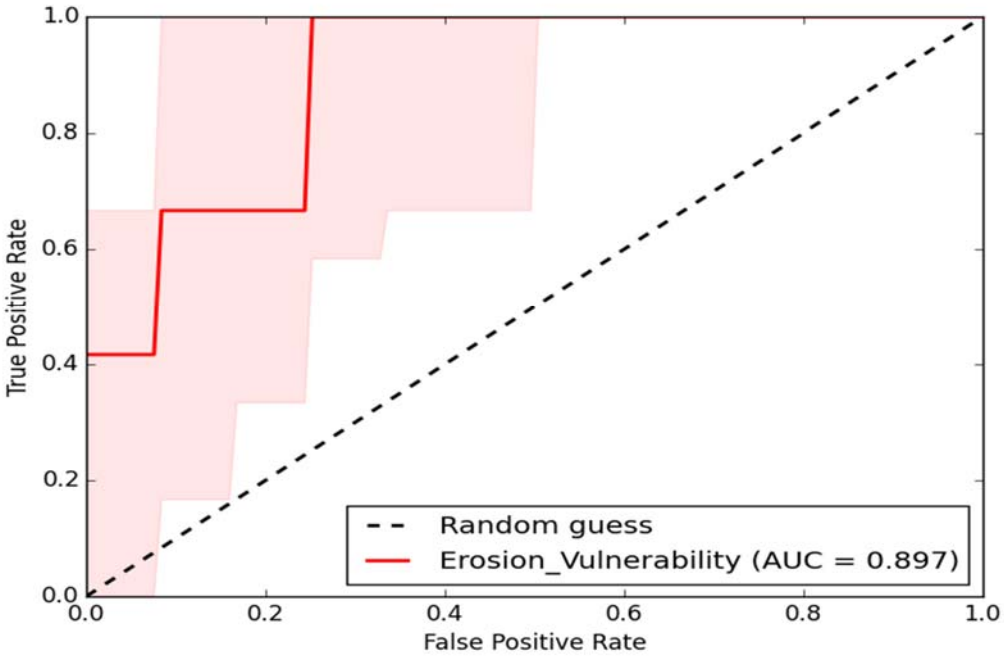

Figure 6: Validation Result of the IVFRN-DEMATEL-ANP Model

Conclusion

This work aimed at investigating the use of a hybrid MCDM model in a GIS environment to assess the vulnerability to erosion hazard based on nine risk factors of Rainfall Erosivity Index,

SPI, STI, TWI, Soil, Land Use, NDVI, Slope and Elevation. The integration of the IVFRN and DEMATEL methods enabled the evaluation of the degree of influence of the risk factors and it was observed that rainfall erosivity index is the most significant factor of erosion hazard in the study area. The result of the aforementioned integration was used as input to apply the ANP method and the relative weights of the risk factors was determined. GIS was employed to delineate the map layers of the considered risk factors and integrate them based on the weighted linear combination method to generate a spatial distribution of erosion hazard vulnerability, a case study area of Anambra state was used to validate the outcome . The resultant vulnerability map reveals that the study area is prone to erosion hazards with 45% of the total area falling into Very High, High and Medium categories of vulnerability. It thus follows that there is a considerable likelihood of increased erosion processes in these areas as climate change continues to intensify hazards. The results also show that Orumba North and Orumba South are the most vulnerable LGAs in the state. The model employed for vulnerability assessment was validated using the AUC-ROC method and an AUC value of 0.897 was obtained to show the model has good predictive performance. With an accuracy of 89.7%, the model has proved to be a viable option for assessing soil erosion vulnerability in data-scarce regions. The study was able to ascertain the feasibility of employing the three methods of IVFRN, DEMATEL and ANP as an assessment model in erosion vulnerability study. It is however recommended that the efficiency of this model should be studied in comparison to other MCDM models. The assessment model identified hydrological and topographical factors as the major cause of erosion hazards in the study area. Hence, the provision of adequate drainage systems is recommended as a means to mitigate erosion hazard in the state. Furthermore, activities that lead to the removal of vegetation and the disturbance of the soil structure should be largely discouraged to aid the control of erosion hazard in the state. The study observed certain limitations in obtaining the pairwise comparison matrix as experts encountered certain difficulties in using fuzzy triple numbers to describe the influence of the factors on one another. Despite this challenge, the method adopted in this study can be a useful tool for producing erosion vulnerability maps to aid soil management and conservation practices.

REFERENCE

Ahmad SNNB, Mustafa FB, Yusoff YM, Didams G (2020) A systematic review of soil erosion control practices on the agricultural land in Asia. International Soil and Water Conservation Research 8:103–115. https://doi.org/10.1016/j.iswcr.2020.04.001

Ajibade FO, Nwogwu NA, Adelodun B, Abdulkadir TS, Ajibade F, Lasisi KH, Fadugba OG, Owolabi TA, Olajire OO (2020) Application of RUSLE integrated with GIS and remote sensing techniques to assess soil erosion in Anambra state, south-eastern Nigeria. Journal of Water and Climate Change 11(1):407–422. https://doi.org/10.2166/wcc.2020.222

Andualem TG, Hagos YG, Kefale A, Zelalem B (2020) Soil erosion prone area identification using multi-criteria decision analysis in Ethiopian highlands. Modeling Earth Systems and Environment 6(3):1407–1418. https://doi.org/10.1007/s40808-020-00757-2

Arabameri A, Pradhan B, Rezaei K, Conoscenti C (2019) Gully erosion susceptibility mapping using GIS-based multi-criteria decision analysis techniques. Catena 180:282–297. https://doi.org/10.1016/j.catena.2019.04.032

Aslam B, Maqsoom A, Salah W, Ali M, Jabbar T, Zafar A (2021) Soil erosion susceptibility mapping using a GIS-based multi-criteria decision approach: case of district Chitral, Pakistan. Ain Shams Engineering Journal 12(2):1637–1649. https://doi.org/10.1016/j.asej.2020.09.015

Bashir IY, Sallau RO, Sheikh AD, Aminu Z, Hassan SM (2020) GIS-based MCDA for gully vulnerability mapping using AHP techniques. Journal of Geographical Studies 4(2):45–63. https://doi.org/10.21523/gcj5.20040201

Borrelli P, Alewell C, Alvarez P, Alexandre J, Anache A, Baartman J, Ballabio C, Bezak N, Biddoccu M, Cerdà A, Chalise D, Chen S, Chen W, Maria A, Girolamo D, Desta G, Deumlich D, Diodato N, Efthimiou N, Panagos P (2021) Soil erosion modelling: a global review and statistical analysis. Science of the Total Environment 780:146494. https://doi.org/10.1016/j.scitotenv.2021.146494

Chalise D, Kumar L, Kristiansen P (2019) Land degradation by soil erosion in Nepal: a review. Soil Systems 3(12):1–18. https://doi.org/10.3390/soilsystems3010012

Chibuzor SN, Okoyeh EI, Egboka BCE, Onwuemesi AG (2020) Gullying processes in the upper idemili river catchment area of Anambra state, Nigeria. Asian Journal of Geological

Research 3(4):64–78.

Das B, Bordoloi R, Thungon LT, Paul A, Pandey PK, Mishra M, Tripathi OP (2020) An integrated approach of GIS, RUSLE And AHP to model soil erosion in west kameng watershed, Arunachal Pradesh. Journal of Earth System Science 129(94):1–18. https://doi.org/10.1007/s12040-020-1356-6

Dike BU, Agunwamba JC, Alakwem O (2015) GIS-based multi-criteria evaluation (MCE) approach for assessment of Urualla gully erosion watershed. Education:2018.

Eekhout JPC, Vente JD (2022) Global impact of climate change on soil erosion and potential for adaptation through soil conservation. Earth-Science Reviews 226:103921. https://doi.org/10.1016/j.earscirev.2022.103921

Egboka BCE, Orji AE, Nwankwoala HO (2019) Gully erosion and landslides in southeastern Nigeria: causes, consequences and control measures. Global Journal of Engineering Sciences 2(4):1–11. https://doi.org/10.33552/GJES.2019.02.000541

Egwuonwu GN, Okoyeh EI, Chikwelu EE (2019) 2DNear-surface litho-structural geophysical investigation at the vicinities of two gully-erosion/landslide sites in south-eastern Nigeria. IOSR Journal of Applied Geology and Geophysics 7(5):70–75. https://doi.org/10.9790/0990-0705017075

Enekwechi E. E. (2017) Effects of pollution and contamination of water bodies: a case of Anambra state. African Journal of Education, Science and Technology 3(4):41–47.

Fagbohun BJ, Olabode OF, Olufemi A, Akinluyi FO (2017) GIS-based sub-basin scale identification of dominant runoff processes for soil and water management in Anambra area of Nigeria. Contemp Trends Geosci 6(2):80–93. https://doi.org/10.1515/ctg-2017-0007

Guo L, Liu R, Men C, Wang Q, Miao Y, Shoaib M, Wang Y, Jiao L, Zhang Y (2021) Multiscale spatiotemporal characteristics of landscape patterns, hotspots, and influencing factors for soil erosion. Science of the Total Environment 779:146474. https://doi.org/10.1016/j.scitotenv.2021.146474

Guo Y, Peng C, Zhu Q, Wang M, Wang H, Peng S (2019) Modelling the impacts of climate and land use changes on soil water erosion: model applications, limitations and future challenges. Journal of Environmental Management 250:109403. https://doi.org/10.1016/j.jenvman.2019.109403

Haidara I, Tahri M, Maanan M, Hakdaoui M (2019) Efficiency of fuzzy analytic hierarchy

process to detect soil erosion vulnerability. Geoderma 354:113853. https://doi.org/10.1016/j.geoderma.2019.07.011

Halefom A, Teshome A, Sisay E, Dananto M (2018) Erosion sensitivity mapping using GIS and multi-criteria decision approach in ribb watershed upper blue nile, Ethiopia. International Journal of Energy and Environmental Science 3(6):99–111. https://doi.org/10.11648/j.ijees.20180306.11

Hatefi SM, Tamošaitienė J (2019) An integrated fuzzy DEMATEL-ANP model for evaluating construction projects by considering interrelationships among risk factors. Journal of Civil Engineering and Management 25(2):114–131.

Hategekimana Y, Yu L, Nie Y, Zhu J, Liu F, Guo F (2018) Integration of multi-parametric fuzzy analytic hierarchy process and GIS along the UNESCO world heritage: a flood hazard index, Mombasa County, Kenya. Natural Hazards 92(2):1137–1153. https://doi.org/10.1007/s11069-018-3244-9

Igwe PU, Ezeukwu JC, Edoka NE, Ejie OC, Ifi GI (2017) A review of vegetation cover as a natural factor to soil erosion. International Journal of Rural Development, Environment and Health Research 1(4):21–28. https://doi.org/10.22161/ijreh.1.4.4

Iliyasu AM, Buba YA, Timnan N, Emeson S, Oyekeshi N (2019) Environmental effects of gully erosion in nigeria case study of Nanka community, orumba north LGA of Anambra state. Journal of Environment and Earth Science 9(10):68–82. https://doi.org/10.7176/JEES/9-10-08

Isife TC (2019) Environmental challenges and protection practices among women of anaocha LGA of Anambra state, Nigeria. African Journal of Sustainable Development 7(3):137–149.

Jin F, Yang W, Fu J, Li Z (2021) Effects of vegetation and climate on the changes of soil erosion in the loess plateau of China. Science of the Total Environment 773:145514. https://doi.org/10.1016/j.scitotenv.2021.145514

Kadoic N, Divjak B, Redep NB (2019) Integrating the DEMATEL with the analytic network process for effective decision-making. Central European Journal of Operations Research 7(3):653–678. https://doi.org/10.1007/s10100-018-0601-4

Kanani-Sadat Y, Arabsheibani R, Karimipour F, Nasseri M (2019) A new approach to flood susceptibility assessment in data-scarce and ungauged regions based on GIS-based hybrid multi criteria decision-making method. Journal of Hydrology 572:17–31.

https://doi.org/10.1016/j.jhydrol.2019.02.034

Mezie EO, Nwajuaku AI (2020) Investigation into the causes of gully erosion in parts of Anambra state. Journal of Science and Technology Research 2(1):139–149.

Mosavi A, Golshanc M, Janizadehd S, Choubine B, Dineva AA, Melesse AM (2022) Ensemble models of GLM, FDA, MARS, and RF for flood and erosion susceptibility mapping: a priority assessment of sub-basins. Geocarto International 37(9):2541–2560.

Mosavi A, Sajedi-Hosseini F, Choubin B, Taromideh F, Rahi G, Dineva AA (2020). Susceptibility mapping of soil water erosion using machine learning models. Water, 12(7):1995. https://doi.org/10.3390/w12071995

Mushi CA, Ndomba PM, Trigg MA, Tshimanga RM, Mtalo F (2019) Assessment of basin-scale soil erosion within the congo river basin: a review. Catena 178:64–76. https://doi.org/10.1016/j.catena.2019.02.030

Nwobodo CE, Otunwa S, Ohagwu VA, Enibe DO (2018) Farmers use of erosion control measures in Anambra state, Nigeria. Journal of Agricultural Extension 22(3):174–184. https://doi.org/10.4314/jae.v22i3.17

Obioji JN, Eze KT (2019) Disaster management in Nigeria: a study of Anambra State, 2011-2019. International Journal of Innovative Development and Policy Studies 7(4):83–103.

Odunuga S, Ajijola A, Igwetu N, Adegun O. (2018) Land susceptibility to soil erosion in orashi catchment, nnewi south, Anambra state, Nigeria. Proc. IAHS 376:87–95. https://doi.org/10.5194/piahs-376-87-2018

Ogbonnaya I, Ugwuoke IJ, Onwuka S, Ozioko O (2020) GIS-based gully erosion susceptibility modeling, adapting bivariate statistical method and AHP approach in Gombe town and environs northeast Nigeria. Geoenvironmental Disasters 7(32):1–16. https://doi.org/10.1186/s40677-020-00166-8

Okonufua E, Olajire OO, Ojeh VN (2019) Flood vulnerability assessment of afikpo south LGA, Ebonyi state, Nigeria. International Journal of Environment and Climate Change 9(6):331–342. https://doi.org/10.9734/IJECC/2019/v9i630118

Okoyeh EI, Akpan AE, Egboka BCE, Okeke HI (2014) An assessment of the influences of surface and subsurface water level dynamics in the development of gullies in Anambra state, southeastern Nigeria. Earth Interactions 18(4):1–24. https://doi.org/10.1175/2012EI000488.1

Pamučar D, Ćirović G, Božanić D (2019) Application of interval valued fuzzy-rough numbers in multi-criteria decision making: the IVFRN-MAIRCA model. Yugoslav Journal of Operations Research 29(2):221–247. https://doi.org/10.2298/YJOR180415011P

Pamucar D, Mihajlovic M, Obradovic R, Atanaskovic, P (2017) Novel approach to group multi-criteria decision making based on interval rough numbers: hybrid DEMATEL-ANP-MAIRCA model. Expert Systems With Applications 88:58–80. https://doi.org/10.1016/j.eswa.2017.06.037

Pamučar D, Petrović I, Ćirović G (2018) Modification of the best–worst and MABAC methods: a novel approach based on interval-valued fuzzy-rough numbers. Expert Systems with Applications 91:89–106. https://doi.org/10.1016/j.eswa.2017.08.042

Peng Q, Wang R, Jiang Y, Zhang W, Liu C (2022) Soil erosion in qilian mountain national park: dynamics and driving mechanisms. Journal of Hydrology: Regional Studies 42:101144. https://doi.org/10.1016/j.ejrh.2022.101144

Rahman RM, Shi ZH, Chongfa C, Dun Z (2015) Assessing soil erosion hazard- a raster based GIS approach with spatial principal component analysis (SPCA). Earth Science Informatics 8(4):853–865. https://doi.org/10.1007/s12145-015-0219-1

Roy J, Pamučar D, Kar S (2020) Evaluation and selection of third party logistics provider under sustainability perspectives: an interval valued fuzzy-rough approach. Annals of Operations Research 293(2): 669-714. https://doi.org/10.1007/s10479-019-03501-x

Saha S, Gayen A, Pourghasemi HR, Tiefenbacher JP (2019) Identification of soil erosion susceptible areas using fuzzy logic and analytical hierarchy process modeling in an agricultural watershed of burdwan district, India. Environmental Earth Sciences 78(23):1–18. https://doi.org/10.1007/s12665-019-8658-5

Saini SS, Jangra R, Kaushik SP (2015) Vulnerability assessment of soil erosion using geospatial techniques- a pilot study of upper catchment of markanda river. International Journal of Advancement in Remote Sensing, GIS and Geography 3(1):9–21.

Sajedi-Hosseini F, Choubin B, Solaimani K, Cerdà A, Kavian A (2018) Spatial prediction of soil erosion susceptibility using FANP: application of the fuzzy DEMATEL approach. Land Degradation and Development 29(9):3092–3103. https://doi.org/10.1002/ldr.3058

Song W, Zhu Y, Zhao Q (2020) Analyzing barriers for adopting sustainable online consumption: a rough hierarchical DEMATEL method. Computers & Industrial Engineering 140(37):

106279. https://doi.org/10.1016/j.cie.2020.106279

Tamene L, Le QB (2015) Estimating soil erosion in sub-saharan Africa based on landscape similarity mapping and using the revised universal soil loss equation (RUSLE). Nutrient Cycling in Agroecosystems 102(1):17-31. https://doi.org/10.1007/s10705-015-9674-9

Wang Y, Hong H, Chen W, Li S, Pamucar D, Gigovic L, Drobnjak S, Bui DT, Duan H (2019) A hybrid GIS multi-criteria decision-making method for flood susceptibility mapping at Shangyou, China. Remote Sensing 11(1):62. https://doi.org/10.3390/rs11010062

Xiong M, Sun R, Chen L (2019) A global comparison of soil erosion associated with land use and climate type. Geoderma 343:31–39. https://doi.org/10.1016/j.geoderma.2019.02.013

APPENDICES

QUESTIONNAIRE FOR EROSION MODELLING IN ANAMBRA STATE

The purpose of this survey is to determine the degree of influence each conditioning factor (criteria) of Erosion has on the other. For this survey, we will consider 9 factors of erosion and they include Rainfall Erosivity (C_1), Stream Power Index (C_2), Sediment Transport Index (C_3), Topographic Wetness Index (C_4), Soil (C_5), Land Use (C_6), Normalized Difference Vegetation Index (C_7), Slope (C_8) and Elevation (C_9). In Table 2, please state the degree of influence the *i*th factor has on the *j*th factor with respect to erosion occurrence. The scale of evaluation in Table 1 below will be used for this evaluation.

Table 1

Linguistic values	Corresponding fuzzy triples
No Influence (NO)	(0, 0, 0.25)
Very Low Influence (VL)	(0, 0.25, 0.5)
Low Influence (L)	(0.25, 0.5, 0.75)
High Influence (H)	(0.5, 0.75, 1.0)
Very High Influence (VH)	(0.75, 1.0, 1.0)

1

Table 2

i \ j	C_1	C_2	C_3	C_4	C_5	C_6	C_7	C_8	C_9
C_1	0, 0, 0.25								
C_2		0, 0, 0.25							
C_3			0, 0, 0.25						
C_4				0, 0, 0.25					
C_5					0, 0, 0.25				
C_6						0, 0, 0.25			
C_7							0, 0, 0.25		
C_8								0, 0, 0.25	
C_9									0,0, 0.25

Each factor has no influence on itself, hence $C_1 - C_1$ is 0, 0, 0.25 and $C_2 - C_2$ is 0, 0, 0.25 and so forth and so on.

Thanks for your time and effort as you participate in this survey.

NAME OF EXPERT:
FIELD:
YEARS OF EXPERIENCE:

2

Appendix 1: Sample of the Questionnaire for Erosion Modelling

	C_1	C_2	C_3	C_4	C_5	C_6	C_7	C_8	C_9
C_1	0,0,0.25	0.25,0.5,0.75	0.5,0.75,1.0	0.25,0.5,0.75	0, 0, 0.25	0.25,0.5,0.75	0, 0, 0.25	0.75,1.0,1.0	0.75,1.0,1.0
C_2	0.25, 0.5,0.75	0, 0, 0.25	0.5, 0.75, 1.0	0.75,1.0,1.0	0,0.25,0.5	0,0.25,0.5	0.25, 0.5,0.75	0.75,1.0,1.0	0.5, 0.75, 1.0
C_3	0.5, 0.75, 1.0	0.75,1.0,1.0	0, 0, 0.25	0.75,1.0,1.0	0.25, 0.5,0.75	0.75,1.0,1.0	0.25, 0.5,0.75	0.75,1.0,1.0	0.75,1.0,1.0
C_4	0.25,0.5,0.75	0.25, 0.5,0.75	0.25, 0.5,0.75	0, 0, 0.25	0.5, 0.75, 1.0	0.5, 0.75, 1.0	0.5, 0.75, 1.0	0.75,1.0,1.0	0.5, 0.75, 1.0
C_5	0, 0, 0.25	0.25, 0.5,0.75	0.25, 0.5,0.75	0.25, 0.5,0.75	0, 0, 0.25	0.5, 0.75, 1.0	0.5, 0.75, 1.0	0.75,1.0,1.0	0.75,1.0,1.0
C_6	0.25, 0.5,0.75	0.5, 0.75, 1.0	0.5, 0.75, 1.0	0.5, 0.75, 1.0	0.5, 0.75, 1.0	0, 0, 0.25	0.75,1.0,1.0	0.75,1.0,1.0	0.75,1.0,1.0
C_7	0, 0, 0.25	0.5, 0.75, 1.0	0.5, 0.75, 1.0	0.5, 0.75, 1.0	0.5, 0.75, 1.0	0.5, 0.75, 1.0	0,0, 0.25	0.75,1.0,1.0	0.75,1.0,1.0
C_8	0.75,1.0,1.0	0.75,1.0,1.0	0.75,1.0,1.0	0.75,1.0,1.0	0.75,1.0,1.0	0.75,1.0,1.0	0.75,1.0,1.0	0,0, 0.25	0.75,1.0,1.0
C_9	0.75,1.0,1.0	0.75,1.0,1.0	0.75,1.0,1.0	0.75,1.0,1.0	0.75,1.0,1.0	0.75,1.0,1.0	0.75,1.0,1.0	0.75,1.0,1.0	0,0, 0.25

Appendix 2: Initial Pairwise Comparison Matrix of Expert 1

	C_1	C_2	C_3	C_4	C_5	C_6	C_7	C_8	C_9
C_1	0, 0, 0.25	0, 0.25, 0.5	0,0.25, 0.5	0,0.25, 0.5	0.25,0.5, 0.75	0.25,0.5, 0.75	0.5, 0.75, 1.0	0.75, 1.0, 1.0	0.75, 1.0, 1.0
C_2	0, 0.25, 0.5	0, 0, 0.25	0,0.25, 0.5	0,0.25, 0.5	0.25,0.5, 0.75	0.25,0.5, 0.75	0.5, 0.75, 1.0	0.5, 0.75, 1.0	0.75, 1.0, 1.0
C_3	0,0.25, 0.5	0,0.25, 0.5	0, 0, 0.25	0,0.25, 0.5	0.25,0.5, 0.75	0.25,0.5, 0.75	0.5, 0.75, 1.0	0.5, 0.75, 1.0	0.75, 1.0, 1.0
C_4	0,0.25, 0.5	0,0.25, 0.5	0,0.25, 0.5	0, 0, 0.25	0.25,0.5, 0.75	0.25,0.5, 0.75	0.5, 0.75, 1.0	0.5, 0.75, 1.0	0.75, 1.0, 1.0
C_5	0,0.25, 0.5	0,0.25, 0.5	0,0.25, 0.5	0,0.25, 0.5	0, 0, 0.25	0.25,0.5, 0.75	0.5, 0.75, 1.0	0.5, 0.75, 1.0	0.75, 1.0, 1.0
C_6	0,0.25, 0.5	0,0.25, 0.5	0,0.25, 0.5	0,0.25, 0.5	0,0.25, 0.5	0, 0, 0.25	0.5, 0.75, 1.0	0.5, 0.75, 1.0	0.75, 1.0, 1.0
C_7	0,0.25, 0.5	0,0.25, 0.5	0,0.25, 0.5	0,0.25, 0.5	0,0.25, 0.5	0,0.25, 0.5	0,0, 0.25	0.25,0.5, 0.75	0.5, 0.75, 1.0
C_8	0,0.25, 0.5	0.5, 0.75, 1.0	0.5, 0.75, 1.0	0.5, 0.75, 1.0	0,0.25, 0.5	0,0.25, 0.5	0,0.25, 0.5	0,0, 0.25	0.5, 0.75, 1.0
C_9	0,0.25, 0.5	0.5, 0.75, 1.0	0.5, 0.75, 1.0	0.5, 0.75, 1.0	0,0.25, 0.5	0,0.25, 0.5	0,0.25, 0.5	0,0.25, 0.5	0,0, 0.25

Appendix 3: Initial Pairwise Comparison Matrix of Expert 2

	C_1	C_2	C_3	C_4	C_5	C_6	C_7	C_8	C_9
C_1	0, 0, 0.25	0.5, 0.75, 1.0	0.75, 1.0, 1.0	0.5, 0.75, 1.0	0.75, 1.0, 1.0	0.5, 0.75, 1.0	0, 0.25, 0.5	0, 0.25, 0.5	0.5, 0.75, 1.0
C_2	0.5, 0.75, 1.0	0, 0, 0.25	0.75, 1.0, 1.0	0.5, 0.75, 1.0	0.5, 0.75, 1.0	0.5, 0.75, 1.0	0, 0.25, 0.5	0.75, 1.0, 1.0	0.5, 0.75, 1.0
C_3	0, 0, 0.25	0, 0, 0.25	0, 0, 0.25	0.5, 0.75, 1.0	0.75, 1.0, 1.0	0.75, 1.0, 1.0	0.5, 0.75, 1.0	0.5, 0.75, 1.0	0.5, 0.75, 1.0
C_4	0, 0, 0.25	0, 0, 0.25	0,0, 0.25	0, 0, 0.25	0.5, 0.75, 1.0	0.5, 0.75, 1.0	0, 0.25, 0.5	0.5, 0.75, 1.0	0, 0.25, 0.5
C_5	0, 0, 0.25	0, 0, 0.25	0,0, 0.25	0, 0, 0.25	0, 0, 0.25	0, 0, 0.25	0, 0, 0.25	0.5, 0.75, 1.0	0.5, 0.75, 1.0
C_6	0, 0, 0.25	0, 0, 0.25	0,0, 0.25	0, 0, 0.25	0, 0, 0.25	0, 0, 0.25	0.5, 0.75, 1.0	0.5, 0.75, 1.0	0.5, 0.75, 1.0
C_7	0, 0, 0.25	0, 0, 0.25	0,0, 0.25	0, 0, 0.25	0, 0, 0.25	0, 0, 0.25	0,0, 0.25	0, 0, 0.25	0,0, 0.25
C_8	0, 0, 0.25	0, 0, 0.25	0,0, 0.25	0, 0, 0.25	0, 0, 0.25	0.5, 0.75, 1.0	0,0, 0.25	0,0, 0.25	0.5, 0.75, 1.0
C_9	0, 0, 0.25	0, 0, 0.25	0,0, 0.25	0, 0, 0.25	0, 0, 0.25	0, 0, 0.25	0, 0, 0.25	0, 0, 0.25	0,0, 0.25

Appendix 4: Initial Pairwise Comparison Matrix of Expert 3

	C_1	C_2	C_3	C_4	C_5	C_6	C_7	C_8	C_9
C_1	(0,0,), (0,0), (0.25,0.25)	(0.13,0.38), (0.38,0.63), (0.63,0.88)	(0.25,0.5), (0.5,0.83), (0.83,1.0)	(0.13,0.38), (0.38,0.63), (0.63,0.88)	(0,0), (0,0.25), (0.25,0.67)	(0.25,0.33), (0.5,0.58), (0.75,0.83)	(0,0), (0,0.25), (0.25,0.58)	(0.5,0.75), (0.75,0.83), (0.83,1.0)	(0.67,0.75), (0.92,1.0), (1.0,1.0)
C_2	(0.13,0.38), (0.38,0.63), (0.63,0.88)	(0,0,), (0,0), (0.25,0.25)	(0.25,0.5), (0.5,0.83), (0.83,1.0)	(0.42,0.67), (0.67,0.83), (0.83,1.0)	(0,0.25), (0.25,0.5), (0.5,0.75)	(0,0.25), (0.25,0.5), (0.5,0.75)	(0.13,0.38), (0.38,0.63), (0.63,0.88	(0.67,0.75), (0.92,1.0), (1.0,1.0)	(0.5,0.58), (0.75,0.83), (1.0,1.0)
C_3	(0.17,0.33), (0.33,0.58), (0.58,1.0)	(0.25,0.42), (0.42,0.58), (0.58,1.0)	(0,0,), (0,0), (0.25,0.25)	(0.42,0.67), (0.67,0.83), (0.83,1.0)	(0.25,0.42), (0.5,0.67), (0.75,0.83)	(0.58,0.75), (0.83,0.92), (0.92,1.0)	(0.25,0.42), (0.5,0.67), (0.75,0.92)	(0.58,0.75), (0.83,1.0), (1.0,1.0)	(0.67,0.75), (0.92,1.0), (1.0,1.0)
C_4	(0.08,0.25), (0.25,0.5), (0.5,0.75)	(0.08,0.25), (0.25,0.5), (0.5,0.75)	(0.08,0.25), (0.25,0.5), (0.5,0.75)	(0,0,), (0,0), (0.25,0.25)	(0.41,0.5), (0.67,0.75), (0.92,1.0)	(0.41,0.5), (0.67,0.75), (0.92,1.0)	(0.33,0.5), (0.58,0.75), (0.83,1.0)	(0.58,0.75), (0.83,1.0), (1.0,1.0)	(0.25,0.5), (0.5,0.83), (0.83,1.0)
C_5	(0,0), (0,0.08), (0.25,0.33)	(0.08,0.25), (0.25,0.5), (0.5,0.75)	(0.08,0.25), (0.25,0.5), (0.5,0.75)	(0.08,0.25), (0.25,0.5), (0.5,0.75)	(0,0,), (0,0), (0.25,0.25)	(0.25,0.42), (0.42,0.67), (0.67,1.0	(0.33,0.5), (0.58,0.75), (0.83,1.0)	(0.58,0.75), (0.83,1.0), (1.0,1.0)	(0.67,0.75), (0.92,1.0), (1.0,1.0)
C_6	(0.08,0.25), (0.25,0.5), (0.5,0.75)	(0.17,0.33), (0.33,0.58), (0.58,1.0)	(0.17,0.33), (0.33,0.58), (0.58,1.0)	(0.17,0.33), (0.33,0.58), (0.58,1.0)	(0.17,0.33), (0.33,0.58), (0.58,1.0)	(0,0,), (0,0), (0.25,0.25)	(0.58,0.75), (0.83,1.0), (1.0,1.0)	(0.58,0.75), (0.83,1.0), (1.0,1.0)	(0.67,0.75), (0.92,1.0), (1.0,1.0)
C_7	(0,0), (0,0.08), (0.25,0.33)	(0.17,0.33), (0.33,0.58), (0.58,1.0)	(0.17,0.33), (0.33,0.58), (0.58,1.0)	(0.17,0.33), (0.33,0.58), (0.58,1.0)	(0.17,0.33), (0.33,0.58), (0.58,1.0)	(0.17,0.33), (0.33,0.58), (0.58,1.0)	(0,0,), (0,0), (0.25,0.25)	(0.33,0.5), (0.5,0.67), (0.67,1.0)	(0.42,0.58), (0.58,0.75), (0.75,1.0)
C_8	(0.25,0.42), (0.42,0.58), (0.58,1.0)	(0.42,0.58), (0.58,0.75), (0.75,1.0)	(0.42,0.58), (0.58,0.75), (0.75,1.0)	(0.42,0.58), (0.58,0.75), (0.75,1.0	(0.25,0.42), (0.42,0.58), (0.58,1.0)	(0.42,0.67), (0.67,0.83), (0.83,1.0)	(0.25,0.42), (0.42,0.58), (0.58,1.0)	(0,0,), (0,0), (0.25,0.25)	(0.58,0.75), (0.83,1.0), (1.0,1.0)
C_9	(0.25,0.42), (0.42,0.58), (0.58,1.0)	(0.42,0.58), (0.58,0.75), (0.75,1.0	(0.42,0.58), (0.58,0.75), (0.75,1.0	(0.42,0.58), (0.58,0.75), (0.75,1.0	(0.25,0.42), (0.42,0.58), (0.58,1.0)	(0.25,0.42), (0.42,0.58), (0.58,1.0)	(0.25,0.42), (0.42,0.58), (0.58,1.0)	(0.25,0.42), (0.42,0.58), (0.58,1.0)	(0,0,), (0,0), (0.25,0.25)

Appendix 5: Interval Value Fuzzy Rough Numbers for Expert 1

	C_1	C_2	C_3	C_4	C_5	C_6	C_7	C_8	C_9
C_1	(0,0,), (0,0), (0.25,0.25)	(0,0.25), (0.25,0.5), (0.5,0.75)	(0,0.25), (0.25,0.5), (0.5,0.83)	(0,0.25), (0.25,0.5), (0.5,0.75)	(0.13,0.25), (0.25,0.5), (0.5,0.88)	(0.25,0.33), (0.5,0.58), (0.75,0.83)	(0.17,0.33), (0.33,0.58), (0.58,1.0)	(0.5,0.75), (0.75,0.83), (0.83,1.0)	(0.67,0.75), (0.92,1.0), (1.0,1.0)
C_2	(0,0.25), (0.25,0.5), (0.5,0.75	(0,0,), (0,0), (0.25,0.25)	(0,0.25), (0.25,0.5), (0.5,0.83)	(0,0.25), (0.25,0.5), (0.5,0.83)	(0.13,0.38), (0.38,0.63), (0.63,0.88)	(0.13,0.38), (0.38,0.63), (0.63,0.88)	(0.125,0.5), (0.5,0.75), (0.75,1.0)	(0.5,0.67), (0.75,0.92), (1.0,1.0)	(0.58,0.75), (0.83,1.0), (1.0,1.0)
C_3	(0,0.13), (0.13,0.38), (0.38,0.75)	(0,0.13), (0.13,0.38), (0.38,0.75)	(0,0,), (0,0), (0.25,0.25)	(0,0.25), (0.25,0.5), (0.5,0.83)	(0.25,0.42), (0.5,0.67), (0.75,0.83)	(0.25,0.5), (0.5,0.75), (0.75,0.92)	(0.41,0.5), (0.67,0.75), (0.92,1.0)	(0.5,0.58), (0.75,0.83), (1.0,1.0)	(0.67,0.75), (0.92,1.0), (1.0,1.0)
C_4	(0, 0.08), (0.13,0.38), (0.38,0.42)	(0, 0.08), (0.13,0.38), (0.38,0.42)	(0, 0.08), (0.13,0.38), (0.38,0.42)	(0,0,), (0,0), (0.25,0.25)	(0.25,0.41), (0.5,0.67), (0.75,0.92)	(0.25,0.41), (0.5,0.67), (0.75,0.92)	(0.33,0.5), (0.58,0.75), (0.83,1.0)	(0.5,0.58), (0.75,0.83), (1.0,1.0)	(0.42,0.67), (0.67,0.83), (0.83,1.0)
C_5	(0,0), (0.08,0.25), (0.33,0.5)	(0, 0.08), (0.13,0.38), (0.38,0.42)	(0, 0.08), (0.13,0.38), (0.38,0.42)	(0, 0.08), (0.13,0.38), (0.38,0.42)	(0,0,), (0,0), (0.25,0.25)	(0.13,0.25), (0.25,0.5), (0.5,0.88)	(0.33,0.5), (0.58,0.75), (0.83,1.0)	(0.5,0.58), (0.75,0.83), (1.0,1.0)	(0.67,0.75), (0.92,1.0), (1.0,1.0)
C_6	(0, 0.08), (0.13,0.38), (0.38,0.42)	(0,0.13), (0.13,0.38), (0.38,0.75)	(0,0.13), (0.13,0.38), (0.38,0.75)	(0,0.13), (0.13,0.38), (0.38,0.75)	(0,0.13), (0.13,0.38), (0.38,0.75)	(0,0,), (0,0), (0.25,0.25)	(0.5,0.58), (0.75,0.83), (1.0,1.0)	(0.5,0.58), (0.75,0.83), (1.0,1.0)	(0.67,0.75), (0.92,1.0), (1.0,1.0)
C_7	(0,0), (0.08,0.25), (0.33,0.5)	(0,0.13), (0.13,0.38), (0.38,0.75)	(0,0.13), (0.13,0.38), (0.38,0.75)	(0,0.13), (0.13,0.38), (0.38,0.75)	(0,0.13), (0.13,0.38), (0.38,0.75)	(0,0.13), (0.13,0.38), (0.38,0.75)	(0,0,), (0,0), (0.25,0.25)	(0.13,0.25), (0.25,0.5), (0.5,0.88)	(0.25,0.38), (0.38,0.75), (0.75,1.0)
C_8	(0,0.13), (0.13,0.38), (0.38,0.75)	(0.25,0.38), (0.38,0.75), (0.75,1.0)	(0.25,0.38), (0.38,0.75), (0.75,1.0)	(0.25,0.38), (0.38,0.75), (0.75,1.0)	(0,0.13), (0.13,0.38), (0.38,0.75)	(0,0.25), (0.25,0.5), (0.5,0.83)	(0,0.13), (0.13,0.38), (0.38,0.75)	(0,0,), (0,0), (0.25,0.25)	(0.5,0.58), (0.75,0.83), (1.0,1.0)
C_9	(0,0.13), (0.13,0.38), (0.38,0.75)	(0.25,0.38), (0.38,0.75), (0.75,1.0)	(0.25,0.38), (0.38,0.75), (0.75,1.0)	(0.25,0.38), (0.38,0.75), (0.75,1.0)	(0,0.13), (0.13,0.38), (0.38,0.75)	(0,0.13), (0.13,0.38), (0.38,0.75)	(0,0.13), (0.13,0.38), (0.38,0.75)	(0,0.13), (0.13,0.38), (0.38,0.75)	(0,0,), (0,0), (0.25,0.25)

Appendix 6: Interval Value Fuzzy Rough Numbers for Expert 2

	C_1	C_2	C_3	C_4	C_5	C_6	C_7	C_8	C_9
C_1	(0,0,), (0,0), (0.25,0.25)	(0.25,0.5), (0.5,0.75), (0.75,1.0)	(0.42,0.67), (0.67,0.83), (0.83,1.0)	(0.25,0.5), (0.5,0.75), (0.75,1.0)	(0.33,0,5), (0.5,0.67), (0.67,1.0)	(0.33,0,5), (0.58,0.75), (0.83,1.0)	(0,0.13), (0.13,0.38), (0.38,0.75)	(0,0.25), (0.25,0.5), (0.5,0.83)	(0.5,0.67), (0.75,0.92), (1.0,1.0)
C_2	(0.25,0.5), (0.5,0.75), (0.75,1.0)	(0,0,), (0,0), (0.25,0.25)	(0.42,0.67), (0.67,0.83), (0.83,1.0)	(0.25,0.5), (0.5,0.83), (0.83,1.0)	(0.25,0.5), (0.5,0.75), (0.75,1.0)	(0.25,0.5), (0.5,0.75), (0.75,1.0)	(0,0.25), (0.25,0.5), (0.5,0.75)	(0.67,0.75), (0.92,1.0), (1.0,1.0)	(0.5,0.58), (0.75,0.83), (1.0,1.0)
C_3	(0,0,), (0,0.25), (0.25,0.58)	(0,0,), (0,0.25), (0.25,0.58)	(0,0,), (0,0), (0.25,0.25)	(0.25,0.5), (0.5,0.83), (0.83,1.0)	(0.42,0.67), (0.67,0.83), (0.83,1.0)	(0.58,0.75), (0.83,0.92), (0.92,1.0)	(0.41,0.5), (0.67,0.75), (0.92,1.0)	(0.5,0.58), (0.75,0.83), (1.0,1.0)	(0.5,0.67), (0.75,0.92), (1.0,1.0)
C_4	(0,0,), (0,0.25), (0.25,0.5)	(0,0,), (0,0.25), (0.25,0.5)	(0,0,), (0,0.25), (0.25,0.5)	(0,0,), (0,0), (0.25,0.25)	(0.41,0.5), (0.67,0.75), (0.92,1.0)	(0.41,0.5), (0.67,0.75), (0.92,1.0)	(0,0.25), (0.25,0.5), (0.5,0.83)	(0.5,0.58), (0.75,0.83), (1.0,1.0)	(0,0.25), (0.25,0.5), (0.5,0.83)
C_5	(0,0), (0,0.08), (0.25,0.33)	(0,0,), (0,0.25), (0.25,0.5)	(0,0,), (0,0.25), (0.25,0.5)	(0,0,), (0,0.25), (0.25,0.5)	(0,0,), (0,0), (0.25,0.25)	(0,0,), (0,0.25), (0.25,0.67)	(0,0.25), (0.25,0.5), (0.5,0.83)	(0.5,0.58), (0.75,0.83), (1.0,1.0)	(0.5,0.67), (0.75,0.92), (1.0,1.0)
C_6	(0,0,), (0,0.25), (0.25,0.5)	(0,0,), (0,0.25), (0.25,0.58)	(0,0,), (0,0.25), (0.25,0.58)	(0,0,), (0,0.25), (0.25,0.58)	(0,0,), (0,0.25), (0.25,0.58)	(0,0,), (0,0), (0.25,0.25)	(0.5,0.58), (0.75,0.83), (1.0,1.0)	(0.5,0.58), (0.75,0.83), (1.0,1.0)	(0.5,0.67), (0.75,0.92), (1.0,1.0)
C_7	(0,0), (0,0.08), (0.25,0.33)	(0,0,), (0,0.25), (0.25,0.58)	(0,0,), (0,0.25), (0.25,0.58)	(0,0,), (0,0.25), (0.25,0.58)	(0,0,), (0,0.25), (0.25,0.58)	(0,0,), (0,0.25), (0.25,0.58)	(0,0,), (0,0), (0.25,0.25)	(0,0,), (0,0.25), (0.25,0.67)	(0,0,), (0,0.25), (0.25,0.75)
C_8	(0,0,), (0,0.25), (0.25,0.58)	(0,0,), (0,0.25), (0.25,0.75)	(0,0,), (0,0.25), (0.25,0.75)	(0,0,), (0,0.25), (0.25,0.75)	(0,0,), (0,0.25), (0.25,0.58)	(0.25,0.5), (0.5,0.83), (0.83,1.0)	(0,0,), (0,0.25), (0.25,0.58)	(0,0,), (0,0), (0.25,0.25)	(0.5,0.58), (0.75,0.83), (1.0,1.0)
C_9	(0,0,), (0,0.25), (0.25,0.58)	(0,0,), (0,0.25), (0.25,0.75)	(0,0,), (0,0.25), (0.25,0.75)	(0,0,), (0,0.25), (0.25,0.75)	(0,0,), (0,0.25), (0.25,0.58)	(0,0,), (0,0.25), (0.25,0.58)	(0,0,), (0,0.25), (0.25,0.58)	(0,0,), (0,0.25), (0.25,0.58)	(0,0,), (0,0), (0.25,0.25)

Appendix 7: Interval Value Fuzzy Rough Numbers for Expert 3